Journal Pre-proof

miRNA-203b-3p induces acute and chronic pruritus via 5-HTR2B and TRPV4

Francesco De Logu, Roberto Maglie, Mustafa Titiz, Giulio Poli, Lorenzo Landini, Matilde Marini, Daniel Souza Monteiro de Araujo, Gaetano De Siena, Marco Montini, Daniela Almeida Cabrini, Michel Fleith Otuki, Priscila Lúcia Pawloski, Emiliano Antiga, Tiziano Tuccinardi, João Batista Calixto, Pierangelo Geppetti, Romina Nassini, Eunice André

PII: S0022-202X(22)01883-8

DOI: https://doi.org/10.1016/j.jid.2022.08.034

Reference: JID 3536

To appear in: *The Journal of Investigative Dermatology*

Received Date: 9 March 2022

Revised Date: 17 June 2022

Accepted Date: 5 August 2022

Please cite this article as: De Logu F, Maglie R, Titiz M, Poli G, Landini L, Marini M, Monteiro de Araujo DS, De Siena G, Montini M, Cabrini DA, Otuki MF, Pawloski PL, Antiga E, Tuccinardi T, Calixto JB, Geppetti P, Nassini R, André E, miRNA-203b-3p induces acute and chronic pruritus via 5-HTR2B and TRPV4, *The Journal of Investigative Dermatology* (2022), doi: https://doi.org/10.1016/j.jid.2022.08.034.

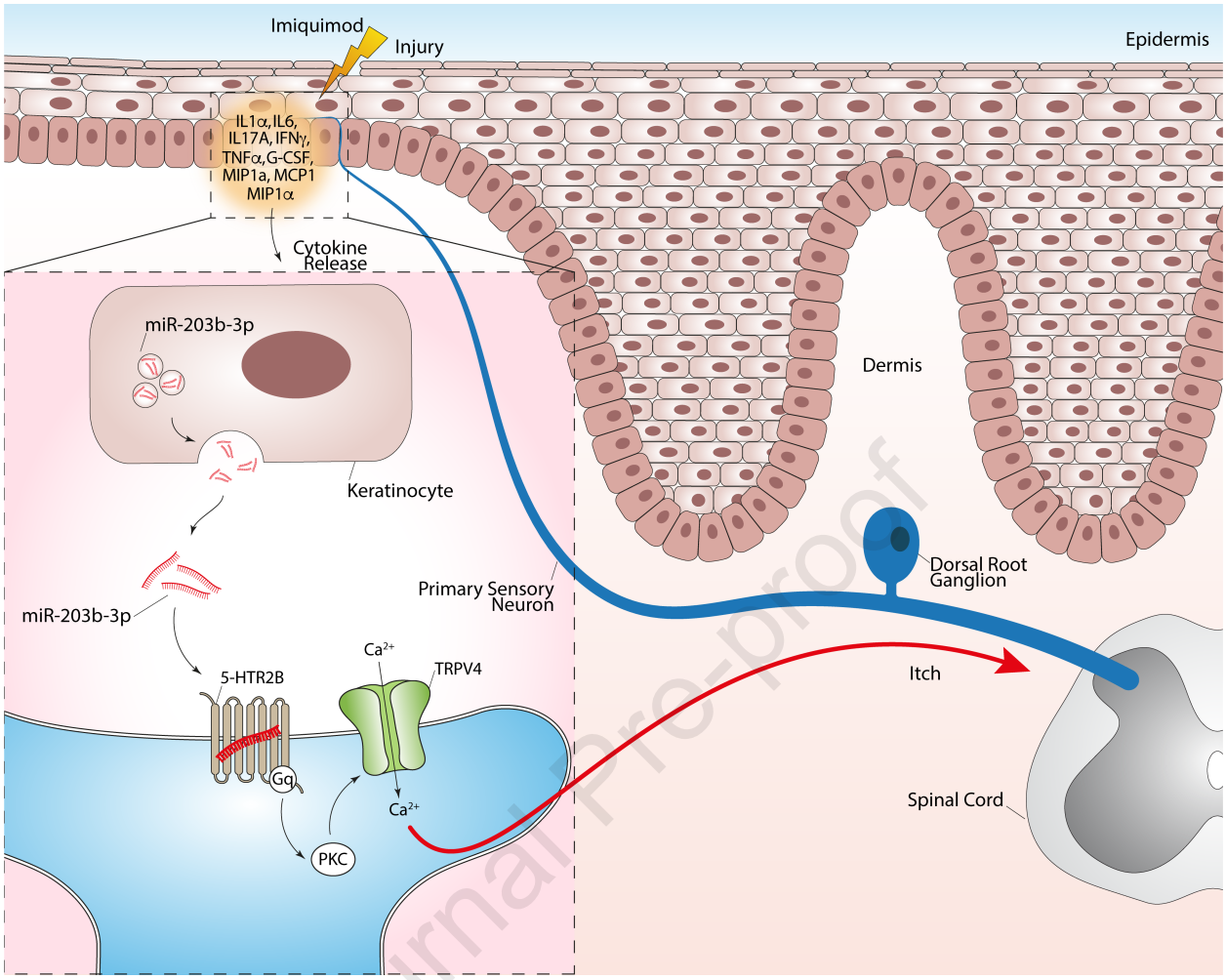

Article type: Original article

miRNA-203b-3p induces acute and chronic pruritus via 5-HTR2B and TRPV4

Francesco De Logu[1], Roberto Maglie[2], Mustafa Titiz[1], Giulio Poli[3], Lorenzo Landini[1], Matilde Marini[1], Daniel Souza Monteiro de Araujo[1], Gaetano De Siena[1], Marco Montini[4], Daniela Almeida Cabrini[5], Michel Fleith Otuki[5], Priscila Lúcia Pawloski[5], Emiliano Antiga[2], Tiziano Tuccinardi[3], João Batista Calixto[6], Pierangelo Geppetti[5], Romina Nassini[1]* and Eunice André[5]

[1]Department of Health Sciences, Section of Clinical Pharmacology and Oncology, University of Florence, 50141, Florence, Italy. [2]Department of Health Sciences, Section of Dermatology, University of Florence, 50141, Florence, Italy. [3]Department of Pharmacy, University of Pisa, 56126 Pisa, Italy. [4]Department of Experimental and Clinical Biomedical Sciences "Mario Serio", Medical Genetics Unit, University of Florence, 50141, Florence, Italy. [5]Department of Pharmacology, Federal University of Paraná, Curitiba, Paraná, 81540-990, Brazil. [6]Centro de Inovação e Ensaios Pré-Clínicos-CIEnP, Florianópolis, Santa Catarina, 88056-000, Brazil

Corresponding author: *Romina Nassini, Department of Health Sciences, Section of Clinical Pharmacology and Oncology, University of Florence, Viale Pieraccini, 6 50139, Florence, Italy Phone +39 055 275 8130, Mobile +39 339 467 2535, Email: romina.nassini@unifi.it; Twitter accounts: @RominaNassini; @UNI_FIRENZE;

Abstract

Growing evidence indicates that transient receptor potential (TRP) channels contribute to different forms of pruritus. However, the endogenous mediators that cause itch *via* TRP channels signaling are poorly understood. Herein, we show that genetic deletion or pharmacological antagonism of TRP vanilloid 4 (TRPV4) attenuated itch in a mouse model of psoriasis induced by topical application of imiquimod. Human psoriatic lesions showed increased expression of several miRNAs, including the miR-203b-3p, which induced a Ca^{2+} response in rodent dorsal root ganglion neurons and scratching behavior in mice *via* serotonin receptor 2B (5-HTR2B) activation and the protein kinase C-dependent phosphorylation of TRPV4. Computer simulation revealed that the miR-203b-3p core sequence (GUUAAGAA) that causes 5-HTR2B/TRPV4-dependent itch, targets the extracellular side of 5-HTR2B by interacting with a portion of the receptor pocket consistent with its activation. Overall, we reveal the unconventional pathophysiological role of an extracellular miRNA that can behave as an itch promoter *via* 5-HTR2B and TRPV4.

Keywords: miRNA, itch, skin diseases, neurons, scratching behavior

Introduction

Pruritus is an unpleasant sensation, i.e., an itch, that leads to the urge to scratch and generally accompanies inflammatory skin diseases. Occasionally, chronic pruritus occurs during the progression of systemic diseases, including liver and renal diseases and various malignancies, significantly impacting patient quality of life (Hashimoto and Yosipovitch, 2019). A subgroup of non-selective Ca^{2+} permeable cation channels, predominantly expressed in a subpopulation of the C- or Aδ-fibers of dorsal root ganglia (DRG) neurons, have received growing interest in a number of physiological and pathophysiological processes, including itch (Caterina and Pang, 2016, Wei et al., 2020, Wilson et al., 2011, Wilson et al., 2013). Namely, the transient receptor potential vanilloid 1 and 4 (TRPV1 and TRPV4, respectively) and TRP ankyrin 1 (TRPA1) are of specific interest regarding itch. For example, TRPV1 and TRPA1 are implicated in signaling the acute and chronic itch evoked by histaminergic and non-histaminergic stimuli (Croce and Calin, 2005, Maglie et al., 2021, Wilson et al., 2011, Xie and Hu, 2018). It has also been reported that TRPV4 can mediate serotonin (5-HT)-induced itch, as around 90% of sensory neurons that respond to 5-HT express TRPV4, and the neuronal response to 5-HT stimulation was reduced by TRPV4 genetic deletion (Akiyama et al., 2016, Snyder et al., 2016).

MicroRNAs (miRNAs) are short, single-stranded, noncoding RNA molecules that are increasingly being investigated for their ability to regulate gene expression by binding to the 3' untranslated regions of cytosolic mRNA targets (Hayes et al., 2014). Recently, an unconventional signaling role of miRNA in itch was identified using a mouse model of cutaneous T-cell lymphoma. Specifically, extracellular miR-711 produced by neoplastic cells promoted a scratching behavior by directly gating the TRPA1 channel (Han et al., 2018). More

recently, a miR-146a was identified as key signaling molecule in cholestatic itch and is released from keratinocytes following TRPV4 stimulation by lysophosphatidylcholine, a precursor of the lysophosphatidic acid (Chen et al., 2021).

We hypothesized that, in addition to cancer and cholestatic pruritus, miRNA dysregulation is mechanistically implicated in itch associated with inflammatory skin diseases. For example, the miRNA signature of psoriasis in skin biopsies has revealed upregulation of a series of miRNAs, including miR-203, miR-184, miR-135b, miR-142-3p, miR-21 and miR-31 (Domingo et al., 2020, Timis and Orasan, 2018). Therefore, we explored which of these miRNAs could mediate itch in a mouse model of psoriasis. Specifically, we found that miR-203b-3p, a keratinocyte-derived miRNA, was able to directly elicit itch in wild-type mice and was critical for itch induction in psoriatic mice *via* activation of the 5-HT receptor 2B (5-HTR2B)/TRPV4 neuronal pathway.

Results

Trpv4 genetic deletion protects from miRNA-203b-3p-induced scratching behavior in mice.

A search for miRNAs that are dysregulated in patients with psoriasis revealed that some miRNAs were upregulated in skin biopsies from psoriatic patients (Domingo et al., 2020). Thus, we tested whether the corresponding mouse miRNA isoforms were capable of provoking a scratching behavior in naive animals following subcutaneous injection in the nape of the neck. Among the eight mouse miRNAs tested (mmu-miR-203b-3p, mmu-miR-203a-5p, mmu-miR-146-5p, mmu-miR-146-3p, mmu-miR-31-3p, mmu-miR-31-5p, mmu-miR-21-3p, mmu-miR-21-5p), only mmu-miR-203b-3p elicited a dose-dependent scratching behavior in naive

mice (Fig. 1a,b). In addition, by using a check model to distinguish itch *vs* pain (Shimada and LaMotte, 2008) we showed that mmu-miR-203b-3p failed to evoke any measurable nociceptive behavior (wiping) at all tested doses (Fig. 1b). As TRPA1, TRPV1, and TRPV4 channels expressed by pruriceptive DRG neurons are implicated in either acute or chronic pruritus (Sun and Dong, 2016), we explored whether mmu-miR-203b-3p triggers the scratching behavior *via* activation of TRP channels. Subcutaneous injection of mmu-miR-203b-3p induced a scratching behavior in *Trpa1*$^{-/-}$ and *Trpv1*$^{-/-}$ similar to the behavior observed in their wildtype littermates (Fig. 1c). However, mmu-miR-203b-3p-induced scratching behavior was absent in *Trpv4*$^{-/-}$ mice (Fig. 1c). As previously reported (Kittaka et al., 2017), we confirm that a TRPV4 agonist, GSK-1016790A (GSK), provoked a dose dependent scratching behavior in mice that was attenuated in mice treated with a TRPV4 antagonist, HC067047 (HC-06) (Fig. S1a) and in *Trpv4*$^{-/-}$ mice (Fig. S1b). Moreover, HC-06 attenuated the scratching behavior elicited by mmu-miR-203b-3p (Fig. S1c).

miR-203b-3p indirectly targets the TRPV4 channel *via* 5-HTR2B.

We next tested whether miR-203b-3p directly gated TRPV4 channels by analyzing the Ca^{2+} response in hTRPV4-HEK293 and mTRPV4-HEK293 cells. While GSK elicited a robust Ca^{2+} response that could be abolished by HC-06, the (human) hsa-miR-203b-3p and mmu-miR-203b-3p failed to elicit any response (Fig. 2a and Fig. S1d). Moreover, hsa-miR-203b-3p failed to evoke any Ca^{2+} response in hTRPV1-HEK293 and hTRPA1-HEK293 cells (Figs S1e,f).

TRPV4 is considered a key downstream component of 5-HT-induced itch (Akiyama et al., 2016) and 5-HTRs were previously shown to induce itch by coupling to TRPV4 channels (Snyder et al., 2016). We confirmed the mRNA expression of various 5-HTR subtypes (Ohta

et al., 2006, Usoskin et al., 2015) and TRPV4 in rat and mouse DRG neurons (De Logu et al., 2020) (Fig. 2b). Moreover, we demonstrated that the rat isoform of miR-203b-3p (rno-miR-203b-3p) induced a concentration-dependent Ca^{2+} response in rat DRGs neurons (Fig. 2c), which was reduced by HC-06 (Fig. 2d). The role of 5-HTR2B was supported by the ability of the selective receptor blocker, ketanserin, to attenuate the rno-miR-203b-3p-induced Ca^{2+} response in rat DRGs neurons (Fig. 2d). 5-HT also elicited a concentration-dependent Ca^{2+} response (Fig. 2e) that was reduced by ketanserin and HC-06 (Fig. 2f). Importantly, HC-06 and ketanserin did not affected the Ca^{2+} response to capsaicin (Fig. 2 and f). The cooperation between 5-HTR2B and TRPV4 was further supported by the failure of mmu-miR-203b-3p, 5-HT and GSK to evoke a Ca^{2+} response in *Trpv4*$^{-/-}$ mouse DRG neurons (Fig. 2g).

Ketanserin inhibited mmu-miR-203b-3p-induced scratching behavior *in vivo*, but did not inhibit GSK-induced scratching behavior (Fig. 2h and Fig. S1g). 5-HT injection caused a dose-dependent scratching behavior (but no wiping behavior) (Fig. 2i), which was attenuated in mice pretreated with both ketanserin and HC-06, and was absent in *Trpv4*$^{-/-}$ mice (Fig. 2j). To exclude the possible role of skin keratinocytes in mmu-miR-203b-3p-induced itch, we tested the Ca^{2+} response induced by mmu-miR-203b-3p in cultured mouse epidermal keratinocytes, isolated from the skin of the back of mice. GSK elicited Ca^{2+} responses, but mmu-miR-203b-3p and 5-HT did not (Fig. 2k). Collectively, these findings confirmed the expression of a functional TRPV4 channel in keratinocytes, and the absence of the 5-HTR2B that would enable these cells to respond to mmu-miR-203b-3p.

miRNA-203b-3p evokes scratching behavior through a conserved eight nucleotide "itching" sequence.

To determine the specific sequence of miR-203b-3p responsible for the scratching behavior, we generated 6 mutants of mmu-miR-203b-3p (m1 to m6) by converting several nucleotides to adenosine (Fig. 3a). These mutants were then injected subcutaneously to test their ability to induce a scratching behavior. The observation that mutations of four nucleotides in m3 and m4 resulted in a markedly reduced effect, led us to identify GUCAAGAA as the "itching" core sequence of mmu-miRNA-203b-3p (Fig. 3b).

A comparison of the mmu-, rno-, and hsa- miR-203b-3p sequences revealed that rno- and hsa- miR-203b-3p contain the same GUUAAGAA core sequence, while the mmu- sequence has a cytosine instead of the second uracil. Interestingly, miR-203b-3p from the 3 species conserved the nucleotide sequence needed to evoke the scratching behavior (Fig. 3c). Specifically, the mouse GUCAAGAA core sequence induced a scratching behavior that was attenuated by HC-06 or ketanserin, and in *Trpv4*$^{-/-}$ mice (Fig. 3d,e). The m1, m2, m5 and m6 core sequences, but not the m3 and m4 sequences, evoked a Ca^{2+} response in mouse DRG neurons (Fig. 2f). The core sequence, as well as GSK, also induced a Ca^{2+} response in *Trpv4*$^{+/+}$ DRGs neurons that are absent in *Trpv4*$^{-/-}$ mice (Fig. 3g).

miR-203b-3p activates mouse 5-HTR2B at the extracellular level.

To evaluate the potential binding complex of murine 5-HTR2B (m5-HTR2B) with the core of sequence of mmu-miRNA-203b-3p, we performed docking studies, combined with molecular dynamics (MD) simulations and binding energy evaluations. The average structure of m5-HTR2B bound to the miRNA core obtained from the last 20 ns of MD simulation is reported

(Fig. 4a). Briefly, the ligand forms extensive interactions with the extracellular side of the receptor, making contact with two extracellular loops (ECL2 and ECL3) and three out of the seven transmembrane (TM) domains (*i.e.,* TM5-TM7). Notably, the adenine of the fourth ribonucleotide (A4) of the miRNA core protrudes significantly within the receptor, thereby occupying the central portion of the extended binding pocket (EBP), which suggests that the miRNA binding conformation is consistent with receptor activation.

Five residues, highlighted in green in Fig. 4A, were primarily predicted to anchor the miRNA core to the extracellular side of the protein through a series of H-bonds. In particular, D350 from the ECL3, which forms H-bonds with the guanine moiety of G6 for almost the whole MD simulation, stabilizes the orientation of the terminal portion of the miRNA core. Meanwhile, D197 from the ECL2 interacted with G1 for most of the MD simulation, especially in the second half, thus fixing the binding conformation of the first three ribonucleotides. The three remaining residues, T209, K210 and K358, contribute to anchor the central portion of the miRNA core to the EBP of the receptor. For most of the MD simulation, the positively charged side chain of K358 is positioned between the phosphate groups of A4 and G6, thus forming H-bonds with the two ribonucleotides (particularly with the phosphate group of G6) that help maintaining the binding conformation of the miRNA core (Fig. 4b). Similarly, T209 and K210 participate in locking the ligand to the protein EBP.

To further assess the interaction of miR-203b-3p and 5-HTR2B, primary cultures of mouse DRGs neurons were incubated with Cy3-labeled mmu-miR-203b-3p. Immunofluorescence results revealed that the Cy3-labeled mmu-miR-203b-3p, but not the scrambled sequence, binds to 5-HTR2B receptors on the cell surface (Fig. 4c), thus confirming their interaction.

Keratinocyte-sensory neuron paracrine signaling mediates the miR-203b-3p and 5-HTR2B/TRPV4-dependent scratching behavior.

To evaluate the pathophysiological implication of miR-203b-3p in psoriatic pruritus (Domingo et al., 2020, Timis and Orasan, 2018), we used a mouse model of psoriasis induced by the topical application of a cream containing IMQ (5%) for 6 consecutive days, as previously described (Horvath et al., 2019, Swindell et al., 2017) (Fig. 5a). Clinical signs of psoriasis measured by the PASI score (*i.e.*, presence of erythema and scales, and increase in skin thickness) were observed in IMQ-treated mice and compared to vehicle-treated (control) mice (Fig. 5b,c), with no difference between male or female mice (Fig. S2a-c). Histological examination confirmed that IMQ-treated mice exhibited a time-dependent increase in epidermal thickness (Fig. 5d). At day 2 after treatment, the mice developed a scratching behavior that persisted until day 7 (Fig. 5e). More importantly, it was found that miR-203b-3p was overexpressed in the psoriatic back skin samples of IMQ-treated mice compared to control mice (Fig. 5f,g), providing evidence of the generation of pruritogenic miR-203b-3p in psoriatic mouse skin samples.

Daily treatment with ketanserin or HC-06, or TRPV4 deletion, attenuated the scratching behavior in IMQ-treated mice without affecting the cumulative PASI score and skin histological changes (Fig. 5h-j). To confirm that miR-203b-3p eventually activates neuronal TRPV4, pSico-AAV2 containing TRPV4-targeted shRNA was injected intrathecally (L4-L6) in *Adv-Cre*$^{+}$ and *Adv-Cre*$^{-}$ mice, to allow for Cre-dependent *Trpv4* gene-silencing specific to sensory neurons (Jung et al., 2016). Both the IMQ treatment and the subcutaneous injection

of mmu-miR-203b-3p induced a scratching behavior in AAV2-*Adv-Cre*$^{-}$ mice that was attenuated in AAV2-*Adv-Cre*$^{+}$ mice (Fig. 6a-c).

It is known that the TRPV4 channel can be activated by protein kinase C (PKC)-dependent phosphorylation (Fan et al., 2009). Therefore, daily treatment with a PKC inhibitor (Ro32-0432) reduced the scratching behavior and skin histological changes evoked by IMQ, but did not reduce the PASI score (Fig. 6d). Moreover, the Ca^{2+} response evoked by mmu-miR-203b-3p in DRG neurons was abated by Ro32-0432 (Fig. 6e). To identify the role of miR-203b-3p in the IMQ-induced scratching behavior, a complementary sequence to mmu-miR-203b-3p was tested and the scratching behavior was reduced by daily subcutaneous injections of this complementary sequence (Fig. 6f).

A considerable number of inflammatory cytokines are increased in psoriatic skin (Chen et al., 2020), including TNFα, IL1α, IL6, and IL17A (Bracke et al., 2013, Grossman et al., 1989, Mee et al., 2007, Tjabringa et al., 2008), and a multiplex array which profiles cytokines in the skin of control and IMQ-treated mice revealed that IL1α, IL2, IL4, IL6, IL10, IL17A, IFNγ, TNFα, M-CSF, G-CSF, MCP1 MIP1α, and MIP1b were increased in skin homogenates of IMQ-treated mice (Fig. 6g). By using an *in vitro* psoriasis model (Bracke et al., 2013), we observed that exposure to a combination of TNFα, IL1α, IL6, and IL17A upregulated miR-203b-3p expression in primary cultures of mouse keratinocytes, but not in DRG neurons (Fig. 6h). These findings suggest that the excitation of neuronal 5-HTR2B/TRPV4 induced by miR-203b-3p occurs *via* a cytokine-mediated miR-203b-3p release from keratinocytes and not through a neuronal autocrine pathway.

Discussion

This study shows that miR-203b-3p, which is upregulated in human psoriatic skin, induced an acute scratching behavior when injected subcutaneously into mice and contributed to sustained itch in a mouse model of psoriasis. These findings extend the proposed unconventional role of miRNAs in pruritogenic signaling that was previously shown for miR-711, which produced itch in a mouse model of cutaneous T-cell lymphoma *via* TRPA1 (Han et al., 2018). More recent results proposed a role for miR-146a in cholestatic pruritus, where release from keratinocytes by a TRPV4-dependent mechanism activates the neuronal TRPV1 (Chen et al., 2021). Our present study provides evidence that neuronal TRPV4, which is over-expressed in chronic itching conditions (Luo et al., 2018), mediates pruritogenic signal induced by miR-203b-3p. This is indicated by the observation that pharmacological blockade, such as total genetic deletion or selective neuronal silencing of TRPV4, protected mice from miR-203b-3p-induced scratching behavior.

Recent studies reported that TRPV4 activation induced itch *via* 5-HT receptors either directly (Luo et al., 2018) or indirectly (Akiyama et al., 2016, Sanjel et al., 2021). Here, we revealed that in pruriceptive neurons, TRPV4 serves as a downstream component of the 5-HTR2B-mediated pathway needed to elicit scratching behavior by miR-203b-3p. Ca^{2+} influx recordings showed that exposure to miR-203b-3p is not sufficient *per se* to induce TRPV4 responses in cells transfected with either human or murine TRPV4, implying that a direct interaction between miR-203b-3p and TRPV4 is unlikely. However, the observation that Ca^{2+} responses by miR-203b-3p or 5-HT were similarly inhibited by 5-HTR2B and TRPV4 antagonism in rodent DRG neurons is consistent with the hypothesis that miR-203b-3p engages an intracellular pathway, which requires the cooperation between 5-HTR2B and

TRPV4. Notably, despite the expression of a functional TRPV4, Ca^{2+} responses were absent in primary cultures of mouse keratinocytes stimulated with miR-203b-3p, supporting the view that miR-203b-3p induces itch *via* direct 5-HTR2B/TRPV4 neuronal signaling without any apparent implication for non-neuronal pathways.

The GUUAAGAA core "itching sequence" is the portion of miR-203b-3p that targets 5-HTR2B and is conserved between different species, as the rat and human sequences were highly homologous with the murine sequence, which differ by just a single nucleotide. In addition, through a computer simulation we predicted the potential interaction sites between miR-203b-3p and the extracellular site of 5-HTR2B consistent with receptor activation. Importantly, our 3D models will facilitate future identification of ligands able to target and inactivate the function of this receptor.

Pruritus represents one of the most troublesome symptoms of psoriasis and affects the quality of life of patients (Hawro et al., 2020, Remrod et al., 2015). The relief from itch is now considered to be an independent benchmark for assessing the efficacy of psoriasis treatments. Similar to other chronic itching conditions including atopic dermatitis, itchy psoriatic skin exhibits high amounts of 5-HT (Komiya et al., 2020). Recently, a role for the TRP canonical 4 (TRPC4) subtype expressed by DRG neurons was reported in 5-HT-induced itch in mice with IMQ-induced psoriasis (Lee et al., 2020). A previous study demonstrated that cutaneous mRNA expression of TRPV4 was downregulated in skin and transiently upregulated in DRG neurons, along with increase in 5-HT expression in the skin of mice in the IMQ model of psoriasis (Li et al., 2014). While we found that genetic deletion or pharmacological antagonism of TRPV4 reduced scratching behavior in the IMQ mouse model of psoriasis, it did not ameliorate the clinical and histologic signs of psoriasis.

Collectively, these findings support the hypothesis that TRPV4 is selectively involved in itch-related pathways, and not in cutaneous psoriatic inflammation.

5-HT was found to sensitize neuronal responses to a selective TRPV4 agonist in mouse DRG neurons, through PKC-dependent pathways (Cenac et al., 2010). Specifically, mice treated with a selective 5-HTR2B antagonist or a PKC inhibitor showed an attenuated scratching behavior, but no reduced inflammation in response to IMQ. This suggested that 5-HTR2B, *via* a PKC pathway, was necessary for TRPV4-induced itch but not skin inflammation. In addition, PKC inhibition reduced Ca^{2+} responses in DRG neurons stimulated with miR-203b-3p, thus confirming the involvement of PKC in the neuronal pruritogenic pathway. While the ability of TRPV4 to induce itch *via* 5-HTR2B has been previously reported (Akiyama et al., 2016, Snyder et al., 2016), here we show that an intracellular pathway that implicates both receptors in DRG neurons mediates pruritus in a mouse model of a major inflammatory skin disease.

Further implications of miRNAs in psoriatic pruritus is provided by the increased expression of various proinflammatory cytokines, and of miR-203b-3p in the skin of the IMQ mouse model of psoriasis. *In vitro* experiments showing that psoriasis-promoting cytokines increased the expression of miR-203b-3p in keratinocytes but not in DRG neurons, support the role of a paracrine pruritogenic signaling pathway. This signaling pathway involves pro-inflammatory cytokines that induce the release of miR-203b-3p from keratinocytes, which targets TRPV4 activation in pruritogenic nerve terminals *via* 5-HTR2B. The anti-pruritogenic effect of a complementary sequence to mmu-miR-203b-3p in the IMQ model highlights the mechanistic relevance of this paracrine pathway in psoriatic itch.

The translational relevance of the present study is two-fold. While previous studies have unraveled the role of miRNAs in itch associated with malignant disease (cutaneous lymphoma) or systemic disease (cholestasis), we herein found that miRNAs promote itch in a mouse model of an inflammatory skin disease. This paves the way for exploring the role of miRNAs in other pruritogenic inflammatory skin diseases, including atopic dermatitis and autoimmune bullous diseases. Second, miR-203b-3p might represent a biomarker and an index of itch severity in psoriasis. Further studies could explore the skin or serum concentrations of miR-203b-3p and their correlation with itch severity, as a diagnostic and prognostic measure. Finally, our study shows that specific targeting of the itching miRNA *via* a complementary sequence attenuates itch in psoriatic mice, thereby highlighting miRNAs as druggable therapeutic targets. A limitation of the present study is that we did not provide evidence that hsa-miRNA evokes pruritus in humans and its implication in human psoriatic itch. However, the observation that not only the murine but also the human core of miR-203b-3p elicited scratching behavior in mice point to the need for testing its ability to produce similar effects in healthy volunteers and to subsequently evaluate the beneficial effects of its complementary sequence in psoriatic patients. The management of pruritus, which is mainly based on corticosteroids and immunosuppressants (Patel and Yosipovitch, 2010), is often unsatisfactory (Stull et al., 2016). The present and previous (Chen et al., 2021, Han et al., 2018) observations offer a therapeutic perspective for a targeted treatment of itch by disease-specific miRNAs.

Materials and Methods

Pharmacological reagents. IMQ cream (5%) was commercially available (Aldara; 3M Pharmaceuticals, UK). If not otherwise indicated, reagents were obtained from Merck Life Science SRL (Milan, Italy).

Animals. Sprague-Dawley (male, 75-100 gr, Charles River RRID_RGD_10395233) rats were used. The following strains of mice were used: C57BL/6J mice (male and female 25-30 g, 5-8 weeks, Charles River, RRID_IMSR_JAX:000664); wild-type (*Trpa1*$^{+/+}$) and TRPA1-deficient (*Trpa1*$^{-/-}$; B6129P-Trpa1^{tm1Kykw}/J; RRID_IMSR_JAX:006401, Jackson Laboratories) mice (Kwan et al., 2006); wild-type (*Trpv1*$^{+/+}$) and TRPV1-deficient (*Trpv1*$^{-/-}$; B6129X1-Trpv1^{tm1Jul}/J, RRID_IMSR_JAX:003770, Jackson Laboratories), wild type (*Trpv4*$^{+/+}$) and TRPV4-deficient (*Trpv4*$^{-/-}$) mice (Liedtke and Friedman, 2003), and *Advillin-Cre* (*Adv-Cre*$^{+}$ and *Adv-Cre*$^{-}$) mice (Guan et al., 2016). Genetically modified mice were all male (25-30 g, 5-8 weeks). The study was approved by the Italian Ministry of Health (research permits #1194/2015-PR) and the Institutional Committee for Animal Care and Use of Federal University of Paraná (protocols number #1234/2018).

Behavioral experiments and treatment protocol, and behavioral assessment for scratching behavior. A detailed description of the method is contained in the Supplementary materials.

Mouse model of psoriasis. Psoriasis model procedure was performed in mice as previously described (van der Fits et al., 2009). Briefly, mice were anesthetized and shaved along their backs the day before the primary IMQ cream application. IMQ cream (62.5 mg) was applied on the shaved back skin daily for 6 consecutive days. Control mice were treated similarly with a vehicle cream (vaseline).

PASI score. A detailed description of the method is contained in the Supplementary materials.

Cell lines, p**rimary culture of rat and mouse DRG neurons and mouse keratinocytes.** A detailed description of the method is contained in the Supplementary materials.

Cell Transfection. The cDNA for the mouse TRPV4 was obtained amplifying the TRPV4 plasmid GFP-tagged in a high transformation efficiency strain of *Escherichia coli* (*DH5α*) with the heat and shock method (Froger and Hall, 2007) and used for transfecting HEK293 cells.

Ca^{2+} **imaging.** A detailed description of the method is contained in the Supplementary materials.

Live cell labeling and immunocytochemistry in mouse DRG neurons. A detailed description of the method is contained in the Supplementary materials.

Fluorescent *in situ* hybridization (FISH). Digoxigenin (DIG)-labeled miRCURY LNA Detection probe (RRID_SCR008539) against mmu-miR-203b-3p (CAGTGGTTCTTGACAGTTCAA), and negative control (GTGTAACACGTCTATACGCCCA) were used for FISH. A detailed description of the method is contained in Supplementary materials.

qRT-PCR. A detailed description of the method is contained in the Supplementary materials.

***In vitro* model of psoriasis.** A detailed description of the method is contained in the Supplementary materials.

Virus Generation. To create the AAV plasmid for the shRNA of mouse TRPV4, a Cre-lox conditional shRNA expression was chosen based on the pSICO system (Ventura et al., 2004). A detailed description of the method is contained in the Supplementary materials.

miRNA measurement by qRT-PCR. RNA was purified from mouse skin samples (50 mg) and from mouse primary culture of keratinocytes and DRG neurons treated with murine IL-1α

(10 ng/ml), recombinant murine IL-6 (5 ng/ml), recombinant murine IL-17A (10 ng/ml) and recombinant murine TNF-α (5 ng/ml). Short RNAs were isolated using the miRVana miRNA isolation kit according to the manufacturer's instructions. A detailed description of the method is contained in the Supplementary materials.

Multi-analyte ELISA assay. A series of chemokines and cytokines including IL-1α, IL-1β, IL-2, IL-4, IL-6, IL-10, IL-12, IL-17A, IFN-γ, TNF-α, M-CSF, G-CSF, GM-GSF, TGF-1β, MCP-1, MIP1α, and MIP1β was assessed in the skin tissue from IMQ and control mice using a multi-analyte ELISA array kit. A detailed description of the method is contained in the Supplementary materials.

Molecular modeling. A detailed description of the method is contained in the Supplementary materials.

Statistical analysis. Results are expressed as mean ± standard error of the mean (SEM). For multiple comparisons, a one-way analysis of variance (ANOVA) followed by the post-hoc Bonferroni's test was used. Two groups were compared using Student's t-test (GraphPad Software Inc.). EC_{50} values and confidence intervals were determined from non-linear regression models. P values less than 0.05 ($P<0.05$) were considered significant. Statistical tests used and the sample size for each analysis are listed in the figure legends.

Data Availability Statement. Materials and raw data generated from this study are available upon request from Romina Nassini (romina.nassini@unifi.it) or Eunice Andre (andreeu@hotmail.com). No large datasets were generated or analyzed during the current study.

Conflicts of Interest: RN, FDL and PG are founding scientists of FloNext Srl. All other authors declare no competing interests

Acknowledgments. Supported by grants from 465430/2014-7/INCT-INOVAMED (EA).

Author Contributions. Conceptualization: FDL, RM, MT, EAn, TT, JBC, PG, RN, EA; Data curation: FDL, RM, MT, EAn, TT, JBC., PG, RN, EA; Formal Analysis: FDL, RM, MT, EAn, TT, JBC., PG, RN, EA; Writing–original draft: FDL, RM, MT, EAn, TT, JBC, PG, RN, EA; Writing–review & editing: FDL, PG, RN, EA; Supervision Funding acquisition: EA; Methodology Writing–original draft GP, LL, MM, DSMdA, GDS., MMo, DAC, MFO, PLP.

References

Akiyama T, Ivanov M, Nagamine M, Davoodi A, Carstens MI, Ikoma A, et al. Involvement of TRPV4 in Serotonin-Evoked Scratching. J Invest Dermatol 2016;136(1):154-60.

Bracke S, Desmet E, Guerrero-Aspizua S, Tjabringa SG, Schalkwijk J, Van Gele M, et al. Identifying targets for topical RNAi therapeutics in psoriasis: assessment of a new in vitro psoriasis model. Arch Dermatol Res 2013;305(6):501-12.

Caterina MJ, Pang ZX. TRP Channels in Skin Biology and Pathophysiology. Pharmaceuticals-Base 2016;9(4).

Cenac N, Altier C, Motta JP, d'Aldebert E, Galeano S, Zamponi GW, et al. Potentiation of TRPV4 signalling by histamine and serotonin: an important mechanism for visceral hypersensitivity. Gut 2010;59(4):481-8.

Chen LL, Deshpande M, Grisotto M, Smaldini P, Garcia R, He ZX, et al. Skin expression of IL-23 drives the development of psoriasis and psoriatic arthritis in mice. Sci Rep-Uk 2020;10(1).

Chen Y, Wang ZL, Yeo M, Zhang QJ, López-Romero AE, Ding HP, et al. Epithelia-sensory neuron crosstalk underlies cholestatic itch induced by lysophosphatidylcholine. Gastroenterology 2021.

Croce CM, Calin GA. miRNAs, cancer, and stem cell division. Cell 2005;122(1):6-7.

De Logu F, Trevisan G, Marone IM, Coppi E, Dalenogare DP, Titiz M, et al. Oxidative stress mediates thalidomide-induced pain by targeting peripheral TRPA1 and central TRPV4. Bmc Biol 2020;18(1).

Domingo S, Sole C, Moline T, Ferrer B, Cortes-Hernandez J. MicroRNAs in Several Cutaneous Autoimmune Diseases: Psoriasis, Cutaneous Lupus Erythematosus and Atopic Dermatitis. Cells-Basel 2020;9(12).

Fan HC, Zhang X, McNaughton PA. Activation of the TRPV4 ion channel is enhanced by phosphorylation. J Biol Chem 2009;284(41):27884-91.

Froger A, Hall JE. Transformation of plasmid DNA into E. coli using the heat shock method. J Vis Exp 2007(6):253.

Grossman RM, Krueger J, Yourish D, Granelli-Piperno A, Murphy DP, May LT, et al. Interleukin 6 is expressed in high levels in psoriatic skin and stimulates proliferation of cultured human keratinocytes. Proc Natl Acad Sci U S A 1989;86(16):6367-71.

Guan Z, Kuhn JA, Wang X, Colquitt B, Solorzano C, Vaman S, et al. Injured sensory neuron-derived CSF1 induces microglial proliferation and DAP12-dependent pain. Nat Neurosci 2016;19(1):94-101.

Han Q, Liu D, Convertino M, Wang Z, Jiang C, Kim YH, et al. miRNA-711 Binds and Activates TRPA1 Extracellularly to Evoke Acute and Chronic Pruritus. Neuron 2018;99(3):449-63 e6.

Hashimoto T, Yosipovitch G. Itching as a systemic disease. J Allergy Clin Immunol 2019;144(2):375-80.

Hawro T, Hawro M, Zalewska-Janowska A, Weller K, Metz M, Maurer M. Pruritus and sleep disturbances in patients with psoriasis. Arch Dermatol Res 2020;312(2):103-11.

Hayes J, Peruzzi PP, Lawler S. MicroRNAs in cancer: biomarkers, functions and therapy. Trends Mol Med 2014;20(8):460-9.

Horvath S, Komlodi R, Perkecz A, Pinter E, Gyulai R, Kemeny A. Methodological refinement of Aldara-induced psoriasiform dermatitis model in mice. Sci Rep-Uk 2019;9.

Jung JY, Lee SE, Hwang EM, Lee CJ. Neuronal Expression and Cell-Type-Specific Gene-Silencing of Best1 in Thalamic Reticular Nucleus Neurons Using pSico-Red System. Exp Neurobiol 2016;25(3):120-9.

Kittaka H, Yamanoi Y, Tominaga M. Transient receptor potential vanilloid 4 (TRPV4) channel as a target of crotamiton and its bimodal effects. Pflug Arch Eur J Phy 2017;469(10):1313-23.

Komiya E, Tominaga M, Kamata Y, Suga Y, Takamori K. Molecular and Cellular Mechanisms of Itch in Psoriasis. Int J Mol Sci 2020;21(21).

Kwan KY, Allchorne AJ, Vollrath MA, Christensen AP, Zhang DS, Woolf CJ, et al. TRPA1 contributes to cold, mechanical, and chemical nociception but is not essential for hair-cell transduction. Neuron 2006;50(2):277-89.

Lee SH, Tonello R, Choi Y, Jung SJ, Berta T. Sensory Neuron-Expressed TRPC4 Is a Target for the Relief of Psoriasiform Itch and Skin Inflammation in Mice. J Invest Dermatol 2020;140(11):2221-+.

Li B, Tsoi LC, Swindell WR, Gudjonsson JE, Tejasvi T, Johnston A, et al. Transcriptome analysis of psoriasis in a large case-control sample: RNA-seq provides insights into disease mechanisms. J Invest Dermatol 2014;134(7):1828-38.

Liedtke W, Friedman JM. Abnormal osmotic regulation in trpv4-/- mice. Proc Natl Acad Sci U S A 2003;100(23):13698-703.

Luo JL, Feng J, Yu G, Yang P, Mack MR, Du JH, et al. Transient receptor potential vanilloid 4-expressing macrophages and keratinocytes contribute differentially to allergic and nonallergic chronic itch. J Allergy Clin Immun 2018;141(2):608-+.

Maglie R, Souza Monteiro de Araujo D, Antiga E, Geppetti P, Nassini R, De Logu F. The Role of TRPA1 in Skin Physiology and Pathology. Int J Mol Sci 2021;22(6).

Mee JB, Johnson CM, Morar N, Burslem F, Groves RW. The psoriatic transcriptome closely resembles that induced by interleukin-1 in cultured keratinocytes: dominance of innate immune responses in psoriasis. Am J Pathol 2007;171(1):32-42.

Ohta T, Ikemi Y, Murakami M, Imagawa T, Otsuguro K, Ito S. Potentiation of transient receptor potential V1 functions by the activation of metabotropic 5-HT receptors in rat primary sensory neurons. J Physiol-London 2006;576(3):809-22.

Patel T, Yosipovitch G. Therapy of pruritus. Expert Opin Pharmaco 2010;11(10):1673-82.

Remrod C, Sjostrom K, Svensson A. Subjective stress reactivity in psoriasis - a cross sectional study of associated psychological traits. Bmc Dermatol 2015;15.

Sanjel B, Kim BH, Song MH, Carstens E, Shim WS. Glucosylsphingosine evokes pruritus via activation of 5-HT(2A) receptor and TRPV4 in sensory neurons. Br J Pharmacol 2021.

Shimada SG, LaMotte RH. Behavioral differentiation between itch and pain in mouse. Pain 2008;139(3):681-7.

Snyder LM, Kuzirian MS, Ross SE. An Unexpected Role for TRPV4 in Serotonin-Mediated Itch. J Invest Dermatol 2016;136(1):7-9.

Stull C, Grossman S, Yosipovitch G. Current and Emerging Therapies for Itch Management in Psoriasis. Am J Clin Dermatol 2016;17(6):617-24.

Sun SH, Dong XZ. Trp channels and itch. Semin Immunopathol 2016;38(3):293-307.

Swindell WR, Michaels KA, Sutter AJ, Diaconu D, Fritz Y, Xing XY, et al. Imiquimod has strain-dependent effects in mice and does not uniquely model human psoriasis. Genome Med 2017;9.

Timis TL, Orasan RI. Understanding psoriasis: Role of miRNAs. Biomed Rep 2018;9(5):367-74.

Tjabringa G, Bergers M, van Rens D, de Boer R, Lamme E, Schalkwijk J. Development and validation of human psoriatic skin equivalents. Am J Pathol 2008;173(3):815-23.

Usoskin D, Furlan A, Islam S, Abdo H, Lonnerberg P, Lou D, et al. Unbiased classification of sensory neuron types by large-scale single-cell RNA sequencing. Nat Neurosci 2015;18(1):145-+.

van der Fits L, Mourits S, Voerman JSA, Kant M, Boon L, Laman JD, et al. Imiquimod-Induced Psoriasis-Like Skin Inflammation in Mice Is Mediated via the IL-23/IL-17 Axis. J Immunol 2009;182(9):5836-45.

Ventura A, Meissner A, Dillon CP, McManus M, Sharp PA, Van Parijs L, et al. Cre-lox-regulated conditional RNA interference from transgenes. Proc Natl Acad Sci U S A 2004;101(28):10380-5.

Wei JJ, Kim HS, Spencer CA, Brennan-Crispi D, Zheng Y, Johnson NM, et al. Activation of TRPA1 nociceptor promotes systemic adult mammalian skin regeneration. Sci Immunol 2020;5(50).

Wilson SR, Gerhold KA, Bifolck-Fisher A, Liu Q, Patel KN, Dong X, et al. TRPA1 is required for histamine-independent, Mas-related G protein-coupled receptor-mediated itch. Nat Neurosci 2011;14(5):595-602.

Wilson SR, Nelson AM, Batia L, Morita T, Estandian D, Owens DM, et al. The ion channel TRPA1 is required for chronic itch. J Neurosci 2013;33(22):9283-94.

Xie ZL, Hu HZ. TRP Channels as Drug Targets to Relieve Itch. Pharmaceuticals-Base 2018;11(4).

Figure legends

Fig. 1. Intradermal miR-203b-3p induces scratching behavior *via* TRPV4. (a) Scratching behavior in C57BL/6J mice was induced by intradermal (i.d., 10 µl) injection of mmu-miR-203b-3p, but not by mmu-miR-203a-5p, mmu-miR-146-5p, mmu-miR-146-3p, mmu-miR-31-3p, mmu-miR-31-5p mmu-miR-21-3p, mmu-miR-21-5p (all, 1 nmol) or vehicle (Veh). **(b)** Dose-dependent scratching behavior and wiping in C57BL/6J mice induced by mmu-miR-203b-3p (0.1-10 nmol, i.d.) or Veh. **(c)** Scratching behavior in *Trpa1*$^{+/+}$ and *Trpa1*$^{-/-}$, *Trpv1*$^{+/+}$ and *Trpv1*$^{-/-}$ or *Trpv4*$^{+/+}$ and *Trpv4*$^{-/-}$ mice induced by mmu-miR-203b-3p (1 nmol, i.d.) or Veh. Mean±SEM, n=4-8 mice per group. **P* < 0.05, *vs.* Veh; §*P*<0.05 *vs.* mmu-miR-203b-3p. One-way ANOVA, Bonferroni correction.

Fig. 2. miR-203b-3p induces TRPV4 activation *via* 5-HTR2B. (a) Typical tracings and cumulative data of the Ca^{2+} response in hTRPV4-HEK293 cells exposed to hsa-miR-203b-3p (10 µM) and GSK-1016790A (GSK, 10 nM) or vehicle (Veh) in the presence of HC-067047 (HC-06, 30 µM) or Veh, (n=4 independent experiments). (**b**) mRNA expression of 5-HTR and TRPV4 in rat and mouse DRG neurons (n=3 independent experiments). Concentration-response curve of the Ca^{2+} response to (**c**) rno-miR-203b-3p and (**e**) 5-HT in rat DRG neurons. Typical tracings and cumulative data of the Ca^{2+} response in rat DRG neurons exposed to (**d**) rno-miR-203b-3p (10 µM) or (**f**) 5-HT (300 µM), capsaicin (CPS, 1 µM) or veh in the presence of HC-06 (30 µM), ketanserin (10 µM) or Veh, and **(g)** mouse DRG neurons from *Trpv4*$^{+/+}$ and *Trpv4*$^{-/-}$ mice exposed to mmu-miR-203b-3p (10 µM), 5-HT (300 µM), CPS (10 µM) or Veh. (n=4 independent experiments). (**h**) Scratching behavior in C57BL/6J mice pretreated (0.5 hr)

with ketanserin (1 mg/kg, intraperitoneal, i.p.) and induced by intradermal (i.d., 10 µl) mmu-miR-203b-3p (1 nmol) or Veh. (**i**) Dose-dependent scratching behavior and wiping in C57BL/6J mice induced by 5-HT (5, 50, 500 nmol, i.d.) or Veh or (**j**) in *Trpv4*$^{+/+}$ pretreated (0.5 hr) with ketanserin (1 mg/kg, i.p.), HC-06 (10 mg/kg, i.p.) or Veh or in *Trpv4*$^{-/-}$ mice (n=6-8 mice per group). **(j)** Typical tracings and cumulative data of the Ca^{2+} response in primary cultures of mouse skin keratinocytes exposed to mmu-miR-203b-3p (10 µM), 5-HT (300 µM), and GSK (100 nM) or Veh (n=4 independent experiments). Dash (-) is the combination of different vehicles. Mean±SEM. **P* < 0.05 *vs.* Veh; §*P*<0.05 *vs.* GSK, rno-miR-203b-3p, 5-HT, mmu-miR-203b-3p. One-way ANOVA, Bonferroni correction.

Fig. 3. miRNA-203b-3p evokes scratching behavior through a conserved core sequence. **(a)** mmu-miR-203b-3p, mutants (m1 to m6), rno-miR-203b-3p, and hsa-miR-203b-3p sequences. Mutated nucleotides are in red, and the core sequence of each miRNA is highlighted in light blue. **(b)** Scratching behavior in C57BL/6J mice induced by intradermal (i.d., 10 µl) mmu-miR-203b-3p (1 nmol), mutants (m1-m6, all 1 nmol) or vehicle (Veh) and **(c)** core sequence of mmu-miR-203b-3p, rno-miR-203b-3p, and hsu-miR-203b-3p (all 1 nmol, i.d.) or Veh. **(d)** Scratching behavior in C57BL/6J mice induced by the core sequence of mmu-miR-203b-3p (1 nmol, i.d.) or Veh and pretreated (0.5 hr) with HC-067047 (HC-06, 10 mg/kg, i.p.), ketanserin (1 mg/kg, i.p.) or Veh and **(e)** in *Trpv4*$^{+/+}$ and *Trpv4*$^{-/-}$ mice (n = 6-8 mice per group). **(f)** Ca^{2+} response in mouse DRG neurons exposed to mmu-miR-203b-3p (10 µM), mutants (m1-m6, 10 µM) or Veh. **(g)** Ca^{2+} response in DRG neurons from *Trpv4*$^{+/+}$ and *Trpv4*$^{-/-}$ mice exposed to the core sequence of mmu-miR-203b-3p (10 µM), GSK-1016790 (GSK, 1 µM) or Veh (n=4 independent experiments). Dash (-) is the combination of different vehicles. Mean±SEM. **P* <

0.05 *vs.* Veh; $^{\S}P<0.05$ *vs.* mmu-miR-203b-3p, core, GSK. One-way ANOVA, Bonferroni correction.

Fig. 4. Computer simulation and immunofluorescence of miRNA-203b-3p binding to 5-HTR2B. (a) Minimized average structure of m5-HTR2B bound to the miRNA core. The phosphate backbone of the miRNA segment is shown as a gold ribbon, ribose is shown in space filling representation, while nucleobases are displayed as blue slabs. The protein surface is shown in gray, while the main miRNA-anchoring residues are shown in green. The orthosteric and extended binding pockets (OBP and EBP, respectively) are indicated together with the three extracellular loops (ECL1-3). **(b)** Detailed interactions formed by the central portion of the miRNA core with the extended binding pocket of m5-HTR2B. The miRNA-anchoring residues T209, K210 and K358 are shown in green, the other proteins are shown in grey. **(c)** Live cell labeling of the binding of Cy3-labeled mmu-miR-203b-3p and Cy3-labeled scramble to 5-HTR2B on the surface of cultured mouse DRG neurons (n=3 replicates, scale bar, 20 μm).

Fig. 5. miR-203b-3p and 5-HTR2B/TRPV4-dependent scratching behavior in a mouse model of itch. (a) Treatment schedule before the behavioral test and tissue sampling in imiquimod (IMQ)-treated or control (CTL, vehicle-treated) mice. **(b)** Representative photographs of the back skin of C57BL/6J mice at day 7 after IMQ or CTL. (**c**) Cumulative PASI score of C57BL/6J mice at day 7 after IMQ or CTL. (**d**) Representative images and cumulative data of the time-dependent (day 0-7) increase in epidermal thickness in C57BL/6J mice after IMQ and (**e**) scratching behavior in C57BL/6J mice after IMQ (scale bar, 20 μm). (**f**) mmu-miR-203b-3 expression relative to cel-mir-39-3p in psoriatic or healthy back skin

samples of C57BL/6J mice at day 7 after IMQ or CTL (n=3 independent experiments). (**g**) Fluorescence *in situ* hybridization of the expression of mmu-mir-203b-3p-Cy3 in psoriatic or healthy back skin samples of C57BL/6J mice at day 7 after IMQ or CTL (n=3 replicates, scale bar, 20 µm). (**h**) Scratching behavior (**i**) cumulative PASI score, and (**j**) epidermal thickness in C57BL/6J mice at day 7 after IMQ or CTL and after the treatment (twice a day from day 1 to day 6) with ketanserin (1 mg/kg, i.p.), HC-067047 (HC-06, 10 mg/kg, i.p.), or Veh and in *Trpv4*$^{+/+}$ and *Trpv4*$^{-/-}$ mice. (n = 6-8 mice per group). Mean±SEM. **P* < 0.05 *vs.* day 0, CTL; §*P*<0.05 *vs.* IMQ. One-way ANOVA, Bonferroni correction.

Fig. 6. Selective primary sensory neurons TRPV4 silencing for the regulation of itch in the imiquimod model, and inflammatory cytokines upregulating miR-203b-3p expression in mouse keratinocytes (a) Representative images of DRG neurons after intrathecal (i.th.) injection with the pSico-AAV2-shRNA (*Trpv4*) viral vector in *Adv-Cre*$^{-}$ and *Adv-Cre*$^{+}$ mice (scale bar, 50 µm). Scratching behavior in *Adv-Cre*$^{-}$ and *Adv-Cre*$^{+}$ mice after injection with the pSico-AAV2-shRNA (*Trpv4*) viral vector (i.th.) **(b)** at day 7 after IMQ or CTL and **(c)** after intradermal (i.d., 10 µl) injection of mmu-miR-203b-3p (1 nmol) or vehicle (Veh). **(d)** Scratching behavior, cumulative PASI score, and epidermal thickness in C57BL/6J mice at day 7 after IMQ or CTL and after treatment with Ro32-0432 (1 mg/kg, i.p.) or Veh. (n = 6 mice per group). **(e)** Typical tracings and cumulative data of the Ca^{2+} response in mouse DRG neurons exposed to mmu-miR-203b-3p (10 µM) or Veh in the presence of Ro32-0432 (100 nM) or Veh, (n=4 independent experiments) (CPS, capsaicin). **(f**) Scratching behavior in C57BL/6J mice at day 7 after IMQ or CTL and mmu-miR-203b-3p inhibitor (1 nmol, i.d.) or Veh (n = 6 mice per group). Mean±SEM. **P* < 0.05 *vs.* CTL; §*P*<0.05 *vs.* IMQ. One-way ANOVA, Bonferroni

correction. **(g)** Cytokines/chemokines array profile in skin samples of C57BL/6J mice at day 7 after IMQ or CTL (n=6 independent experiments). (**h**) Mmu-miR-203b-3p expression relative to cel-mir-39-3p in primary cultures of mouse keratinocytes and DRG neurons exposed to TNFα, IL1α, IL6, and IL17A (n=3 independent experiments). n.d. not detectable. Mean±SEM. **P* < 0.05 *vs.* CTL, veh; §*P*<0.05 *vs.* IMQ. Student's t-test.

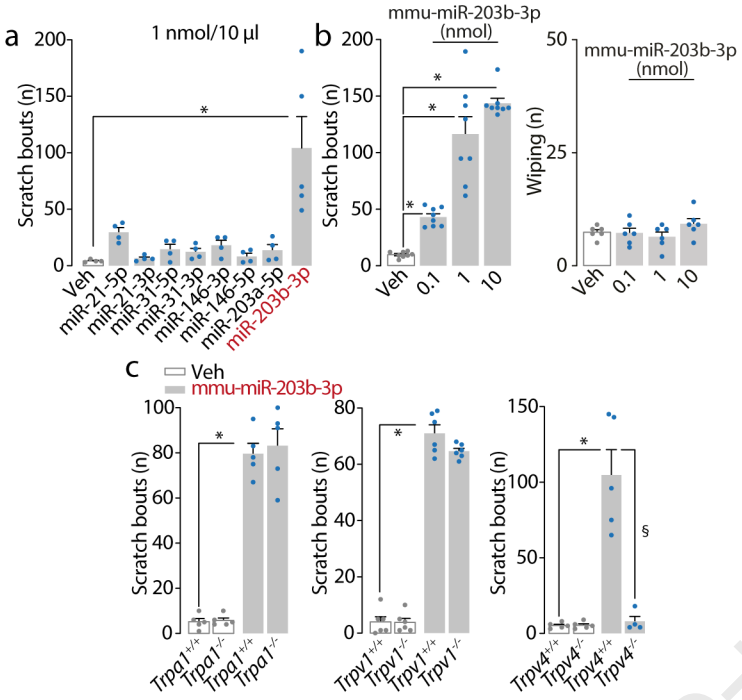

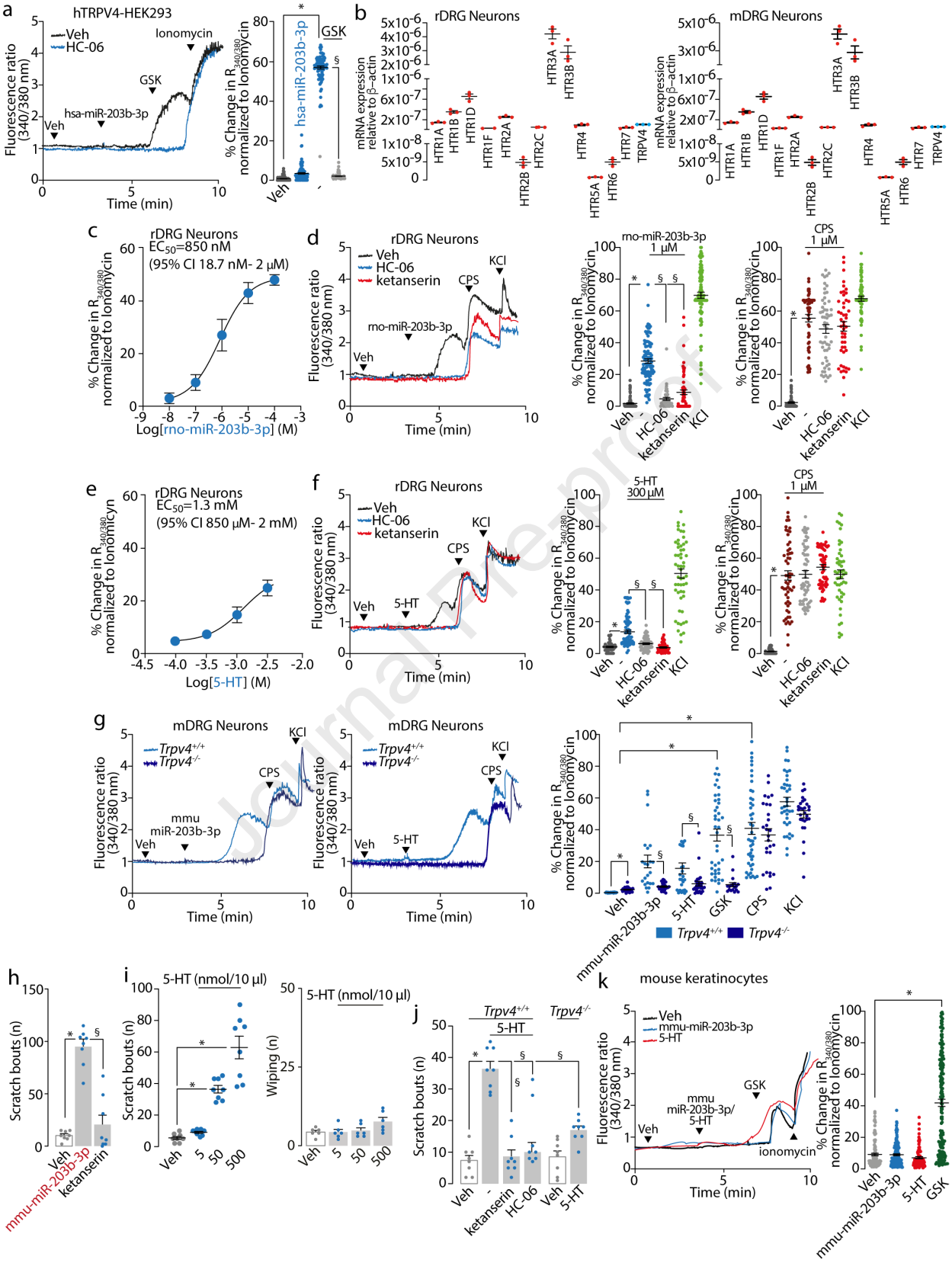
a
hTRPV4-HEK293
Veh
HC-06
Ionomycin
GSK
hsa-miR-203b-3p
Fluorescence ratio (340/380 nm)
Time (min)
% Change in R340/380 normalized to Ionomycin
hsa-miR-203b-3p
GSK
b
rDRG Neurons
mDRG Neurons
mRNA expression relative to β-actin
HTR1A
HTR1B
HTR1D
HTR1F
HTR2A
HTR2B
HTR2C
HTR3A
HTR3B
HTR4
HTR5A
HTR6
HTR7
TRPV4
c
rDRG Neurons
EC50=850 nM
(95% CI 18.7 nM- 2 μM)
% Change in R340/380 normalized to Ionomycin
Log[rno-miR-203b-3p] (M)
d
rDRG Neurons
Veh
HC-06
ketanserin
CPS
KCl
rno-miR-203b-3p
Fluorescence ratio (340/380 nm)
Time (min)
rno-miR-203b-3p
1 μM
CPS
1 μM
Veh
HC-06
ketanserin
KCl
e
rDRG Neurons
EC50=1.3 mM
(95% CI 850 μM- 2 mM)
% Change in R340/380 normalized to Ionomycin
Log[5-HT] (M)
f
rDRG Neurons
Veh
HC-06
ketanserin
CPS
KCl
5-HT
Fluorescence ratio (340/380 nm)
Time (min)
5-HT
300 μM
CPS
1 μM
g
mDRG Neurons
Trpv4+/+
Trpv4-/-
CPS
KCl
mmu miR-203b-3p
5-HT
Fluorescence ratio (340/380 nm)
Time (min)
Veh
mmu-miR-203b-3p
5-HT
GSK
CPS
KCl
h
Scratch bouts (n)
Veh
mmu-miR-203b-3p
ketanserin
i
5-HT (nmol/10 μl)
Scratch bouts (n)
Wiping (n)
Veh
5
50
500
j
Trpv4+/+
Trpv4-/-
5-HT
Scratch bouts (n)
Veh
ketanserin
HC-06
5-HT
k
mouse keratinocytes
Veh
mmu-miR-203b-3p
5-HT
mmu miR-203b-3p/ 5-HT
GSK
ionomycin
Fluorescence ratio (340/380 nm)
Time (min)
% Change in R340/380 normalized to Ionomycin
Veh
mmu-miR-203b-3p
5-HT
GSK

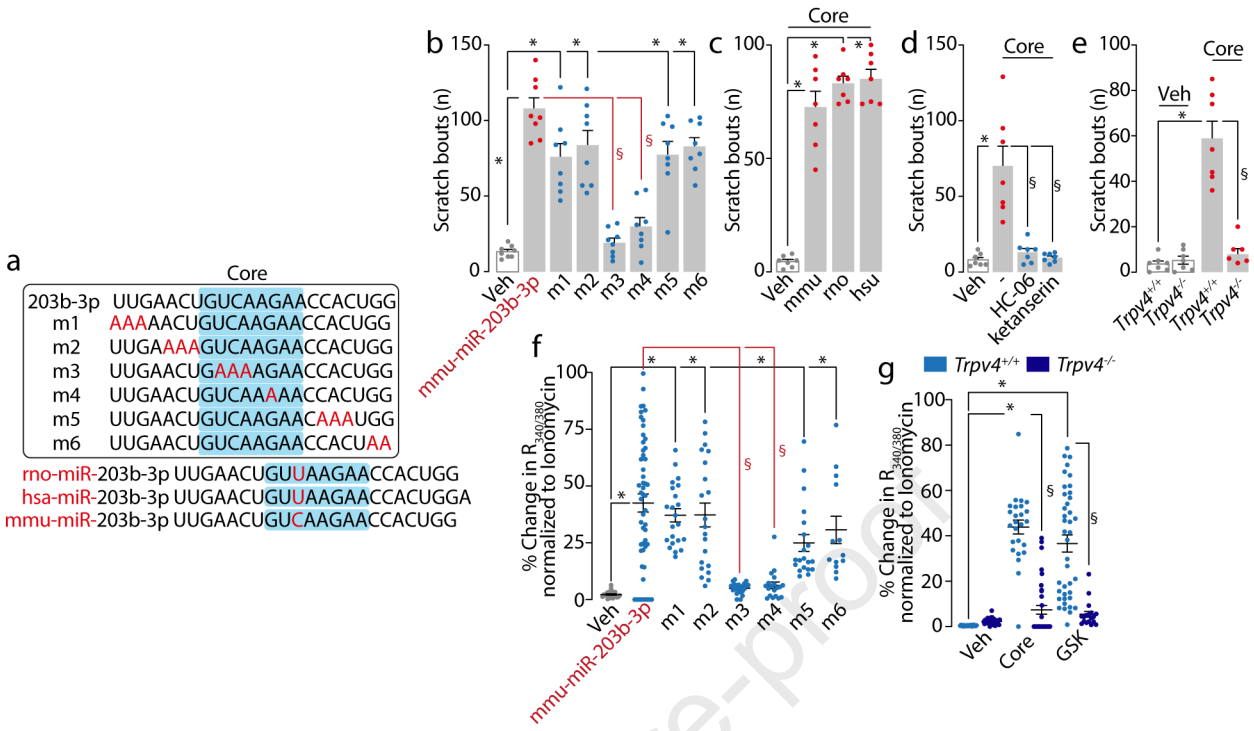

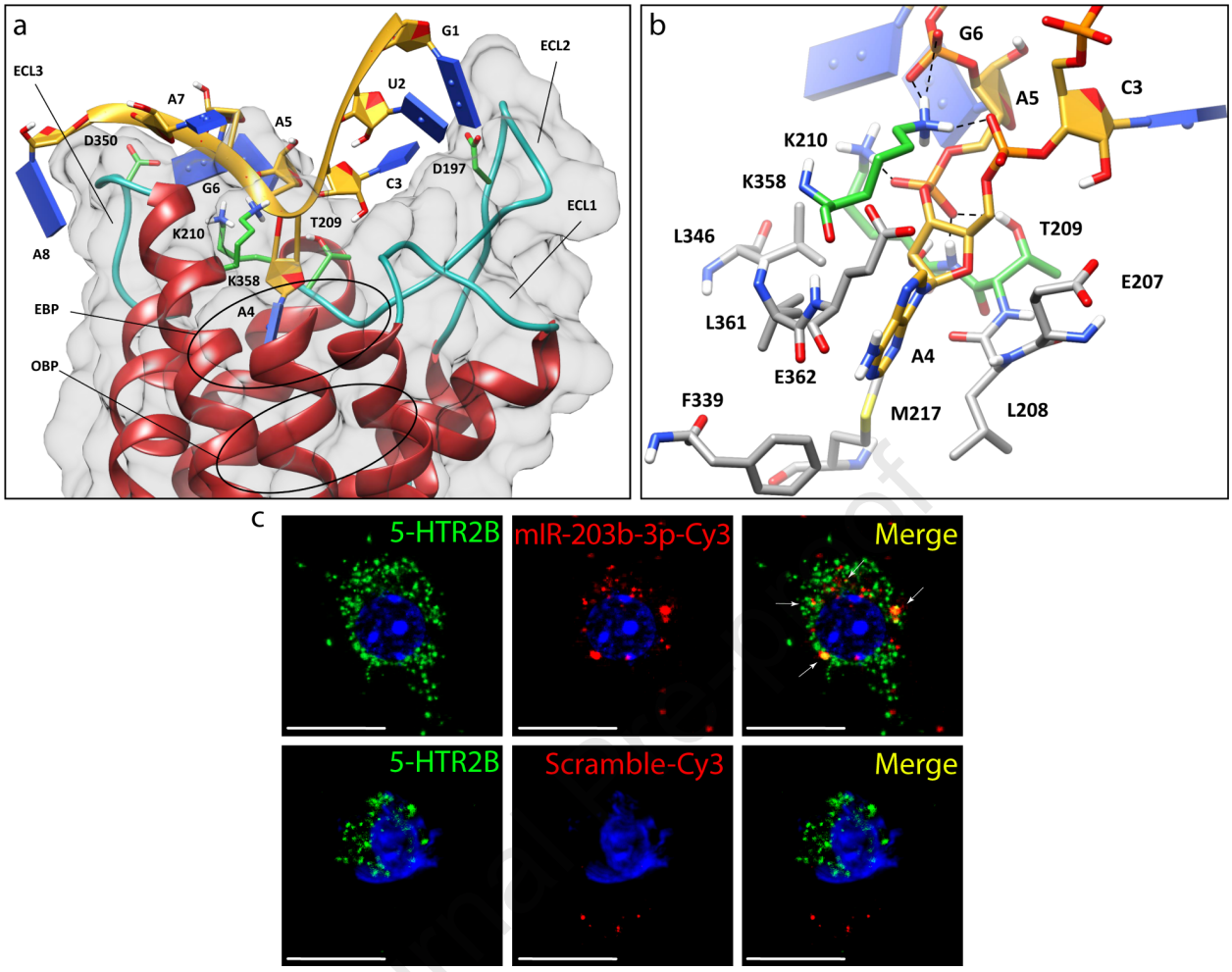

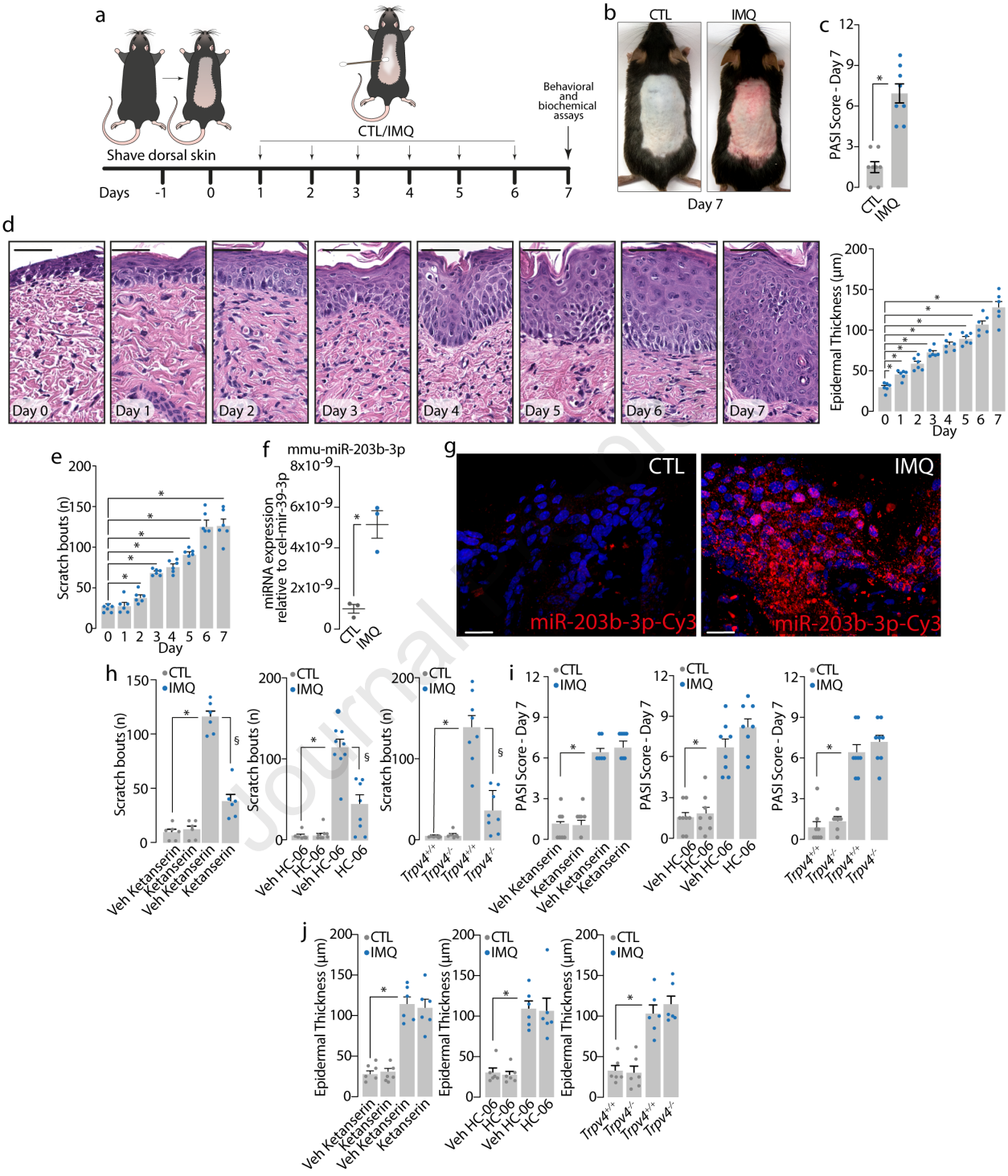
a
Shave dorsal skin
CTL/IMQ
Behavioral and biochemical assays
Days -1 0 1 2 3 4 5 6 7
b
CTL
IMQ
Day 7
c
PASI Score - Day 7
CTL
IMQ
d
Day 0
Day 1
Day 2
Day 3
Day 4
Day 5
Day 6
Day 7
Epidermal Thickness (µm)
Day
e
Scratch bouts (n)
Day
f
mmu-miR-203b-3p
miRNA expression relative to cel-mir-39-3p
CTL
IMQ
g
CTL
IMQ
miR-203b-3p-Cy3
miR-203b-3p-Cy3
h
Scratch bouts (n)
CTL
IMQ
Veh Ketanserin
Ketanserin
Veh HC-06
HC-06
Trpv4+/+
Trpv4-/-
i
PASI Score - Day 7
j
Epidermal Thickness (µm)

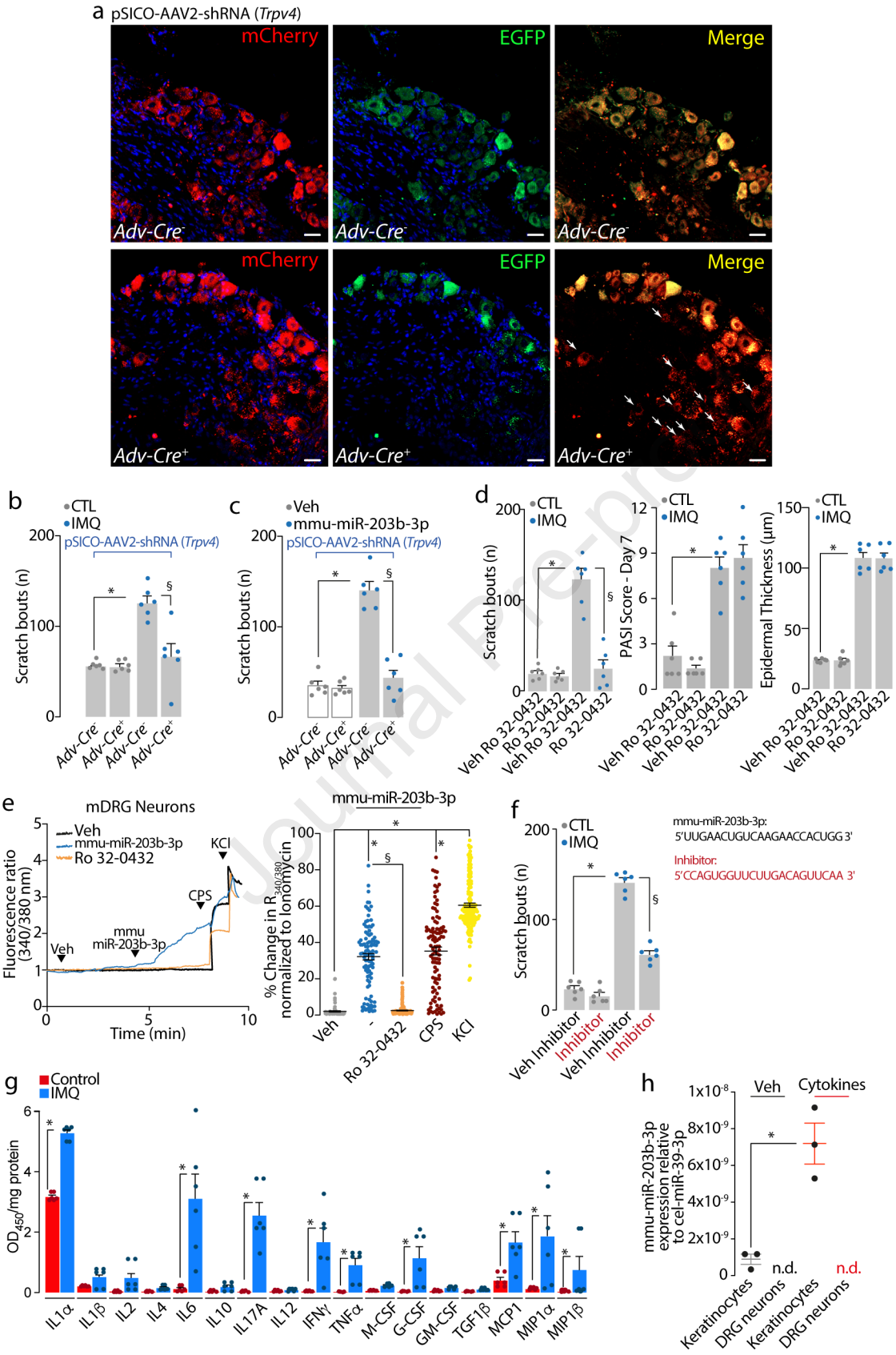
a pSICO-AAV2-shRNA (Trpv4)
mCherry
EGFP
Merge
Adv-Cre-
Adv-Cre+
b
CTL
IMQ
pSICO-AAV2-shRNA (Trpv4)
Scratch bouts (n)
c
Veh
mmu-miR-203b-3p
d
PASI Score - Day 7
Epidermal Thickness (µm)
Veh Ro 32-0432
Ro 32-0432
e
mDRG Neurons
Veh
mmu-miR-203b-3p
Ro 32-0432
KCl
CPS
mmu miR-203b-3p
Fluorescence ratio (340/380 nm)
Time (min)
% Change in R340/380 normalized to Ionomycin
f
mmu-miR-203b-3p:
5'UUGAACUGUCAAGAACCACUGG 3'
Inhibitor:
5'CCAGUGGUUCUUGACAGUUCAA 3'
Veh Inhibitor
Inhibitor
g
Control
IMQ
OD450/mg protein
IL1α
IL1β
IL2
IL4
IL6
IL10
IL17A
IL12
IFNγ
TNFα
M-CSF
G-CSF
GM-CSF
TGF1β
MCP1
MIP1α
MIP1β
h
Veh
Cytokines
mmu-miR-203b-3p expression relative to cel-miR-39-3p
n.d.
Keratinocytes
DRG neurons

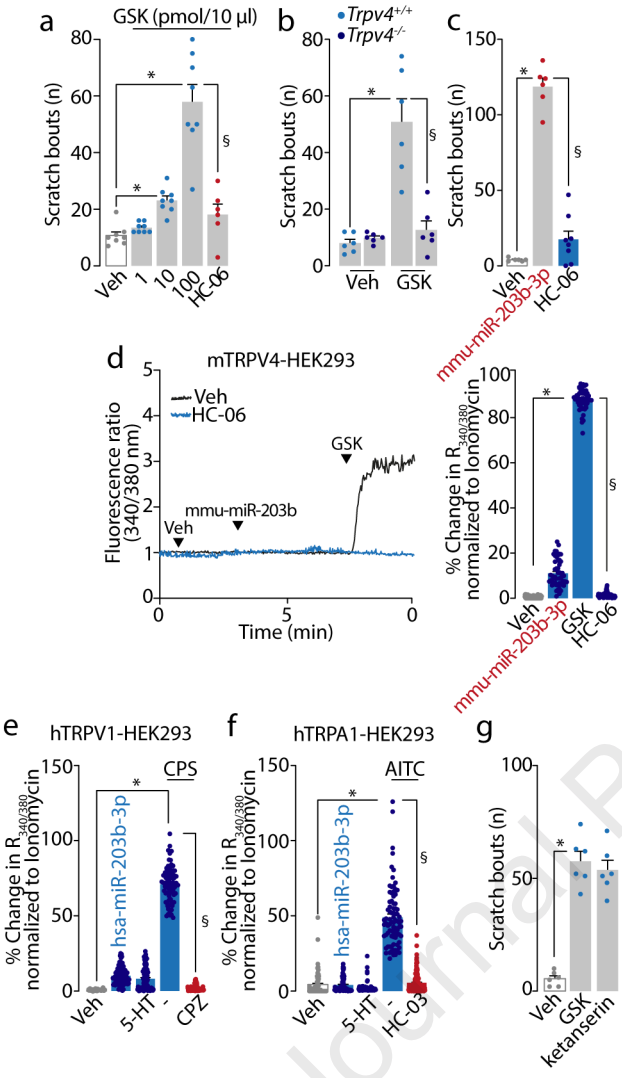

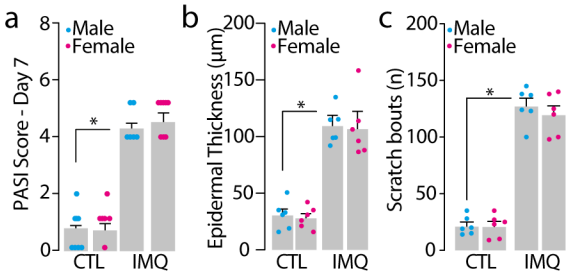

Supplementary materials

Supplementary Methods

Behavioral experiments

All behavioral experiments were in accordance with European Union (EU) guidelines for animal care procedures and the Italian legislation (DLgs 26/2014) application of the EU Directive 2010/63/EU. The behavioral studies followed the animal research reporting *in vivo* experiment (ARRIVE) guidelines (Kilkenny et al., 2010). Mice were housed in a temperature- and humidity-controlled *vivarium* (12 hr dark/light cycle, free access to food and water, 5 animals per cage). At least 1 hr before behavioral experiments, mice were acclimatized to the experimental room and behavior was evaluated between 9:00 am and 5:00 pm. All the procedures were conducted following the current guidelines for laboratory animal care and the ethical guidelines for investigations of experimental pain in conscious animals set by the International Association for the Study of Pain (Zimmermann, 1983).

The group size of n = 4-8 animals for behavioral experiments was determined by sample size estimation using G*Power (v3.1) (Faul et al., 2007) to detect size effect in a post-hoc test with type 1 and 2 error rates of 5 and 20%, respectively. Mice were allocated to vehicle or treatment groups using a randomization procedure (http://www.randomizer.org/). Investigators were blinded to the identities (genetic background) and treatments, which were revealed only after data collection. No animals were excluded from experiments. Animals were anesthetized with a mixture of ketamine and xylazine (90 mg/kg and 3 mg/kg, respectively, i.p.) and euthanized with inhaled CO_2 plus 10-50% O_2.

Treatment protocol. C57BL/6J (IMQ or control mice) were treated with HC-067047 (10 mg/kg, i.p.), ketanserin (1 mg/kg, i.p), Ro 32-0432 (1 mg/kg, i.p.) or their vehicle (4% DMSO, 4% Tween 80 in 0.9% NaCl) twice a day starting from day 1 to day 6 of IMQ or vehicle treatment. C57BL/6J IMQ or control mice were treated with the complementary sequence to mmu-miR-203b-3p (1 nmol, intradermal, i.d., 10 µl, in the nape of the neck) or vehicle (0.9% NaCl) once a day starting from day 1 to day 6 of IMQ or vehicle treatment. C57BL/6J mice were injected (i.d., 10 µl) in the nape of the neck with mmu-miR-203b-3p (0.1, 1 and 10 nmol) and mmu-miR-203a-5p, mmu-miR-146-5p, mmu-miR-146-3p, mmu-miR-31-3p, mmu-miR-31-5p, mmu-miR-21-3p, mmu-miR-21-5p (all, 1 nmol) or vehicle (0.9% NaCl), mmu-miR-203b-3p mutants (m1-m6, all 1 nmol), mmu-miR-203b-3p, rno-miR-203b-3p and hsa-miR-203b-3p core sequence (all, 1 nmol) or vehicle (0.9% NaCl), 5-HT (5, 50 and 500 nmol) or vehicle (0.9% NaCl), and GSK-1016790A (1, 10, 100 pmol) or vehicle (4% DMSO 4%

Tween 80 in 0.9% NaCl). In a different set of experiments C57BL/6J mice were pretreated (0.5 hr before the i.d. application of the different stimuli) with HC-067047 (10 mg/kg, i.p.), ketanserin (1 mg/kg, i.p) or vehicle (4% DMSO 4% Tween 80 in 0.9% NaCl). *Trpa1*$^{+/+}$ and *Trpa1*$^{-/-}$, *Trpv1*$^{+/+}$ and *Trpv1*$^{-/-}$ mice were injected (i.d., 10 µl, in the nape of the neck) with mmu-miR-203b-3p (1 nmol) or vehicle (0.9% NaCl). *Trpv4*$^{+/+}$ or *Trpv4*$^{-/-}$ mice were injected (i.d., 10 µl, in the nape of the neck) with mmu-miR-203b-3p (1 nmol), mmu-miR-203b-3p core sequence (1 nmol) or vehicle (0.9% NaCl), 5-HT (50 nmol), GSK-1016790A (100 pmol/10 ul) or vehicle (4% DMSO 4% Tween 80 in 0.9% NaCl or 0.9% NaCl). Some *Trpv4*$^{+/+}$ mice were pretreated (0.5 hr before 5-HT) with HC-067047 (10 mg/kg, i.p.), ketanserin (1 mg/kg, i.p) or vehicle (4% DMSO 4% Tween 80 in 0.9% NaCl). *Adv-Cre*$^{+}$ or *Adv-Cre*$^{-}$ mice were treated with the intratechal (i.th., 5 µl) injection of pSico-AAV2-shRNA (*Trpv4*) viral vector 4.2 x 10^{12} GC/ml, two weeks before IMQ or vehicle treatment. Some C57BL/6J were injected (i.d., 10 µl) in the cheek with mmu-miR-2 03b-3p (0.1, 1 and 10 nmol) 5-HT (5, 50 and 500 nmol) or vehicle (0.9% NaCl).

Psoriasis area and severity index (PASI) score. The cumulative PASI score included erythema, scales, and thickening evaluation (Luo et al., 2016). Each index was scored independently on a scale from 0 to 4: 0-none, 1-slight, 2-moderate, 3-marked, 4-maximum. The cumulative score (erythema plus scaling plus thickening) was used to measure the severity of inflammation (scale 0-12). The score for each mouse was averaged to observed changes in skin lesions.

Behavioral assessment for scratching behavior and wiping. Mice were placed into plexiglass boxes and videotaped for 60 min. Generally, 3-4 mice were videotaped simultaneously. Immediately after beginning videotaping, all investigators left the room. Videotapes were analyzed by investigators blinded to the treatment and genotype, and the number of scratch and wiping bouts were counted over a 60-min and 30-min period. One bout of scratching was defined as an episode in which a mouse lifted its paw and scratched continuously for any length of time, until the paw was returned to the floor (Wilson et al., 2011). Hind paw movements directed away from the treated area (e.g., ear-scratching) and grooming movements were not counted. A bout of wiping was defined as a continuous wiping movement with a forepaw directing at the area of the injection area (Shimada and LaMotte, 2008).

Cell lines. Human embryonic kidney (HEK293) (#CRL-1573™, American Type Culture Collection) cells were cultured in DMEM supplemented with heat-inactivated FBS (10%), L-glutamine (2 mM),

penicillin (100 U/ml) and streptomycin (10 mg/ml) at 37 °C in 5% CO_2 and 95% O_2. HEK293 cells stably transfected with the cDNA for the human TRPA1 (hTRPA1-HEK293) were cultured in DMEM containing heat-inactivated FBS (10%), L-glutamine (2 mM) and penicillin/streptomycin (100 U/ml), sodium pyruvate (1 mM) and G418 (1 mg/ml). HEK293 cells stably transfected with the cDNA for human TRPV1 (hTRPV1-HEK293) were grown in MEM containing heat-inactivated FBS (10%), L-glutamine (2%), antibiotic/antimycotic solution (2%) and selected with G418 (1µl/ml). HEK293 cells stably transfected with the cDNA for human TRPV4 (hTRPV4-HEK293) were cultured in DMEM containing FBS tetracycline free (10%), hygromycin B (100 µg/ml) and blasticidine S hydrochloride (5 µg/ml). Tetracycline (0.1 µg/ml) was added overnight before calcium imaging experiments. All cells were used when received without further authentication.

Primary culture of rat and mouse dorsal root ganglion (DRG) neurons. DRGs (combined cervical, thoracic, and lumbar) were bilaterally excised under a dissection microscope and enzymatically digested using 2 mg/ml of collagenase type 1A and 1 mg/ml of trypsin, for rat DRG neurons, or 2 mg/ml of collagenase type 1A and 1mg/ml of papain, for mouse DRG neurons, in HBSS for 35 min at 37 °C. Ganglia were disrupted by several passages through a series of syringe needles (23-25G). Rat and mouse neurons were then pelleted by centrifugation at 1200 x rpm for 5 min at room temperature (RT) and resuspended in DMEM supplemented with 10% heat inactivated horse serum (rat DRG neurons) or Ham's-F12 (mouse DRG neurons), both containing 10% heat-inactivated FBS, 100 U/ml of penicillin, 0.1 mg/ml streptomycin and 2 mM L-glutamine added with 100 ng/ml nerve growth factor (NGF) and 2.5 mM cytosine-b-D-arabino-furanoside free base (ARA-C), and maintained at 37 °C in 5% CO_2 and 95% O_2 for 3 days before being used for calcium imaging experiments.

Primary culture of mouse tail keratinocytes. The mouse tail was cut off and the skin was peeled off and cut in smaller pieces (2-3 cm). The peeled skin was digested in 4 mg/ml dispase in keratinocytes growth medium (EpiVita, Cell Applications, Inc) at 4 °C overnight. The day after, tissue was washed in PBS to remove excessed dispase, and the dermis was slowly lifted up and away from the epidermis. The separated epidermis was put and float on drops (500 µl) of trypsin-EDTA solution (0.25%) with the basal layer downward the skin on a petri dish at RT on a horizontal shaker with gentle agitation. After 20 min, keratinocytes growth medium was added to the petri dish and the epidermis was grasped using forceps and vigorously rubbed back and forth to release single cells from the epidermal sheet. These passages were repeated three times. The cell clumps were broken using a serological pipette and then passing the cell solution through a 100 µm filter. The filtered cells were centrifuged for 5 min at 180 x g and seeded in culture dishes precoated with bovine collagen I

(5 μg/ml) and put at 37 °C in 5% CO_2 and 95% O_2 until reaching confluence. Keratinocyte terminal differentiation was induced by adding $CaCl_2$ (0.2 mM) to the culture medium (Li et al., 2017).

Primary culture of mouse epidermal keratinocytes. The dorsal skin (approximately 9 cm^2) of four mice was removed, placed hairy side down in a petri dish and all subcutaneous tissue were scraped under sterile condition. Skin was sliced into 0.5 cm x 1-1.5 cm strips using a scalpel and placed hairy side up on the surface of 20 ml of PBS added with trypsin (0.25%) for 2 h at 32 °C. Floating skin strips were transferred to a new petri dish containing keratinocytes growth medium and the epidermis was scraped off using a scalpel blade and forceps. The medium containing scraped epidermal cells and the skin strips was collected into a sterile 60 ml jar with a magnetic stir bar and stirred at 100 x rpm for 20 min at room temperature. The content was passed through a 70 μm cell strainer filter. The cell filtrate was centrifuged at 160 x g for 7 min at 4 °C, the pellet was resuspended by gently triturating with a 5 ml pipet and cells were plated on 35 mm glass coverslips precoated with bovine collagen I (5 μg/ml) and maintained at 32°C in 5% CO_2 and 95% O_2 for 24 hr (Morris et al., 2019).

Cell Transfection. After reaching 50%-70% confluence in a 24 multiwell plate, cells were incubated with 8.4 μg/ml of plasmid DNA in OptiMEM in presence of transfection reagent *TransIT* (MIRUS Optimization protocol for plasmid DNA delivery) for 72 hr. Transfected cells were grown in MEM containing 10% heat-inactivated FBS, 100 U/ml of penicillin, 0.1 mg/ml of streptomycin plus neomycin 250 μg/ml.

Calcium imaging. Cells were plated on poly-L-lysine-coated (8.3 μM) 35 mm glass coverslips (Thermo Fisher Scientific) and maintained at 37 °C in 5% CO_2 and 95% O_2 for 24 hr. Cells were loaded (40 min) with Fura-2 AM-ester (5 μM) added to the buffer solution (37 °C) containing (in mM) 2 $CaCl_2$; 5.4 KCl; 0.4 $MgSO_4$; 135 NaCl; 10 D-glucose; 10 HEPES and bovine serum albumin (BSA, 0.1%) at pH 7.4. Cells were washed and transferred to a chamber on the stage of a fluorescent microscope for recording (Olympus IX 81, Olympus). hTRPA1-HEK293, hTRPV1-HEK293, hTRPV4-HEK293, mTRPV4-HEK293 cells, rat and mouse DGRs neurons were exposed to has-mmu- and rno- miR -203b-3p (10 nM - 100 μM), 5-HT (10 nM - 3 mM), mmu-miR-203b-3p mutants (m1-m6, all 10 μM), allyl isothiocyanate (10 μM), capsaicin (1 μM-10 μM), GSK1016790A (10 nM - 10 μM) and KCl (50 mM). The Ca^{2+} response was monitored in the presence of ketanserin (10 μM), HC-067047 (30 μM) capsazepine (30 μM) or vehicle (0.1 - 0.3 % DMSO) and Ro 32-0432 (100 nM) or its vehicle (0.001%DMSO) in mouse DRG neurons. A high concentration (50 mM) of KCl that

depolarize functional neurons causing Ca^{2+} influx, was used to further exclude the non-neuronal cells. Mouse epidermal keratinocytes were exposed to mmu-miR-203b-3p (10 μM), GSK1016790A (100 nM), 5-HT (300 μM) or vehicle (0.001%DMSO). Results were expressed as percent increase in ratio 340/380 over baseline normalized to the maximum effect induced by ionomycin (5 μM) added at the end of each experiment.

Live cell labeling and immunocytochemistry in mouse DRG neurons. DRG neurons were plated on poly-L-lysine (8.3 μM) and laminin (5 μM) coated 35 mm glass coverslips (Thermo Fisher Scientific) and maintained at 37 °C in 5% CO_2 and 95% O_2 for 24 hr. Cells were incubated with Cy3-labeled miR-203b-3p or Cy3-scramble-miR-203b-3p-m2 (RRID_SCR_001363), 1 mM diluted in extracellular cell solution, for 15 min at 37 °C in 5% CO_2 and 95% O_2. Coverslips were washed and incubated with 5-HTR2B primary antibody (1:1000, RRID_SCR012931) at RT for 1 hr. The cells were incubated with the fluorescent polyclonal secondary antibody Alexa Fluor 488 (1:600; RRID_SCR008410) and examined with a Zeiss AxioImager2 microscope in a z-stack and Apotome mode (Carl Zeiss Spa, Milan).

Fluorescent *in situ* hybridization (FISH). Anesthetized mice were transcardially perfused with PBS and 4% paraformaldehyde and the skin was dissected and fixed overnight with 4% paraformaldehyde. Frozen sections (14 μm) were washed in PBS added with 0.1% Tween20 (PBT) and acetylated for 10 min with triethanolamine and acetic anhydride to prevents non-specific binding of the probe. Sections were then incubated with proteinase K (1:20000; stock solution 20 μg/μl; RRID_SCR 001326) for 10 min followed by a fixation with 4% paraformaldehyde for 15 min at RT. The tissue was prehybridize in hybridization buffer (HB) at 60°C for 1 hr and the probes were diluted with HB to 50 nM and hybridized at 60°C overnight. Sections were then washed with PBT and blocking solution (RRID_SCR 001326) diluted in maleic acid buffer with Tween 20, 30 min at RT, then incubated with alkaline phosphatase conjugated anti-DIG (1:2000; RRID_SCR 001326) at 4°C overnight. After washing with PBT and alkaline phosphatase inhibition buffer (NTMT, 0.1 M NaCl, 0.1 M Tris-HCl pH 9.5, 0.05 M $MgCl_2$, 0.1 % Tween 20), the *in situ* signals were developed with a fast red substrate (RRID_SCR 001326) (1 tablet in 2 ml 0.1 M Tris-HCl pH 8.2) for 3 hr. Slides were then washed in PBT and cover-slipped using mounting medium with DAPI (RRID_SCR012931). The images were captured by a Zeiss AxioImager2 microscope in a z-stack and Apotome mode (Carl Zeiss Spa, Milan).

qRT-PCR. Total RNA was extracted from mouse and rat DRGs. The standard TRIzol extraction method was used together with RNeasy Mini Kit (RRID_SCR008539) according to the

manufacturer's protocol. RNA concentration and purity were assessed spectrophotometrically by measuring the absorbance at 260 nm 280 nm. The RNA purified from DRGs was reverse transcribed using SuperScript™ IV VILO™ master mix with ezDNase™ enzyme according to manufacturer's protocol. The KAPA SYBR® FAST universal kit was used for the amplification, and the cycling conditions were as follows: samples were heated to 95 °C for 10 min followed by 40 cycles of 95 °C for 10 sec, and 65 °C for 20 sec. PCR reaction was performed in triplicate for each sample. Relative expression of mRNA was calculated using the $2^{-\Delta(\Delta CT)}$ comparative method, with each gene normalized against the β-actin. For relative quantification of mRNA compared to housekeeping gene, real- time PCR was carried out using Rotor Gene Q (Qiagen Spa). The sets of primers for mouse and rat are listed in the Table S3.

Virus Generation. The construct AAV2-EF1-mCherry-SICO-GFP-mTRPV4-shRNA was purchased on Vector BioLabs. The conditional expression of mTRPV4 shRNA (5' CACCGCAACATGCGTGAATTCATCACTCGAGTGATGAATTCACGCATGTTGC TTTTTT-3'; Ref Seq#: NM_022017) is regulated through the recognition of two modified loxP sites (named TATAlox) by *Cre*, which recombines the pSICO vector exciding the CMV-eGFP cassette and flanking the TATAlox-shRNA sequence next to the U6 promoter. The recombination replaces the correct spacing between the promoter and the transcription start site, resulting in the transcription of mTRPV4 shRNA. In the absence of *Cre*, the CMV-eGFP cassette is placed between the U6 promoter and the shRNA transcription start site, avoiding the expression of mTRPV4 shRNA. Otherwise, mCherry expression is constitutive under an EF1 promoter. AAV2 was used at a viral titer of 4.2 x 10^{12} GC/ml (Vector BioLabs).

***In vitro* model of psoriasis.** For *in vitro* model mimicking the psoriasis phenotype mouse primary culture of keratinocytes and DRG neurons were plated in 6-well plates (Thermo Fisher Scientific) and maintained in 5% CO_2 and 95% O_2 (24 hr, 37 °C). The medium was added with recombinant murine IL-1α (10 ng/ml), recombinant murine IL-6 (5 ng/ml), recombinant murine IL-17A (10 ng/ml) and recombinant murine TNF-α (5 ng/ml) and cells were maintained in 5% CO_2 and 95% O_2, overnight, 37 °C, before the extraction and measurement of miRNA by qRT-PCR.

miRNA measurement by qRT-PCR. Briefly, total RNA samples were mixed with 5 volumes of lysis/binding buffer and 1/10 volume of miRNA homogenate additive and left on ice for 10 min. A low concentration of ethanol (25% v/v) was then added to the samples which were subsequently mixed and bound to a filter cartridge by centrifugation. The relatively low concentration of ethanol

in this first treatment allows the binding of the larger RNAs to the column while the shorter, more soluble RNAs pass through and are collected. In the second step, a higher concentration of ethanol was added to the eluant (40% v/v), allowing the shorter RNAs to be immobilized to filter cartridges during centrifugation and subsequently eluted. All RNA samples were immediately used or kept at -80°C until further processing. Reverse transcription reactions were performed using the Taqman Advanced miRNA cDNA Synthesis Kit following the manufacturer's protocol. For mRNA relative quantification, qPCR was performed on Rotor Gene Q (Qiagen, SpA) using TaqMan™ Fast Advanced Master Mix (2x) and TaqMan™ Advanced miRNA Assay specific for mmu-miR-203b-3p (Stem loop Accession #MI0040622) and for cel-miR-39-3p (Stem loop Accession #MI0000010). Relative quantities of miRNAs were calculated using the $2^{-\Delta(\Delta CT)}$ comparative method, after normalization to the spiked-in control *Caenorhabditis elegans* miRNA-39 (cel-miRNA-39).

Multi-analyte ELISA assay. Briefly, skin samples were dissected from euthanized IMQ and control mice, homogenized in PBS (0.1 M) with a tissue homogenizer (Qiagen SpA) for 30 sec, centrifuged at 10000 x g for 10 min, and supernatants were collected and assayed according to the manufacturer's protocol. Samples were assayed in triplicate. The raw data obtained from the absorbance (optical density, OD 450 nm) readings were normalized to the mg of protein.

Molecular modeling

Since no X-ray structure of m5-HTR2B is currently available, a 3D model of the protein was generated based on the X-ray structure of h5-HTR2B in complex with the agonist ligand ergotamine (PDB code 4IB4) (Wacker et al., 2013). The core sequence of the miRNA was docked on the extracellular side of the m5-HTR2B model using Gold software, generating 100 different potential binding modes. The 22 most reliable binding modes selected after a careful visual inspection and post-docking filtering were further analyzed through MD simulation studies. The corresponding miRNA-protein complexes were embedded in a lipid bilayer, solvated with explicit water molecules, and subjected to an MD protocol including a three-step energy minimization, brief heating and equilibration stages, and a final production stage of 25 to 50 ns of MD simulation. The 7 most stable complexes in terms of root-mean-square deviation (RMSD) of the miRNA core during the MD were then analyzed from an energetic point of view, by performing miRNA-protein binding free energy evaluations using the Molecular Mechanics - Poisson-Boltzmann Surface Area (MM-PBSA) approach. The obtained results strongly suggested complex 11 as the most energetically favored one, since the binding energy associated to this complex (-78.5 kcal/mol) was significantly better than those associated to the other complexes (Table S1). Based on the whole computational analysis,

complex 11, which also showed the lowest miRNA RMSD value during the whole 50 ns of MD simulation (average RMSD = 4.4 Å, Table S2), was considered as the most reliable miRNA-protein complex.

Protein structure refinement and modeling. Molecular modeling studies were performed using a model of murine 5-HTR2B receptor (m5-HTR2B) generated based on the X-ray structure of the human 5-HTR2B (h5-HTR2B), as the two isoforms presented more than 80% sequence identity. Considering the hydrophilic nature of miRNAs and the presence of a well-known ligand-binding site located on the extracellular side of 5-HTR2B, which can accommodate various small-molecule ligands endowed with agonist activity, we envisioned that the miRNA core could interact with m5-HTR2B on its extracellular side, occupying at least part of the ligand binding pocket. Based on these considerations, the X-ray structure of h5-HTR2B in complex with ergotamine (PDB code 4IB4) (McCorvy et al., 2018), was selected as a reference. In fact, ergotamine interacts with a wide portion of the extracellular side of the receptor, encompassing both the supposed orthosteric binding pocket (OBP), buried within the transmembrane protein region and occupied by the ergoline core of the ligand, and a shallower region occupied by the benzyltripeptide moiety of the agonist that can be referred to as extended binding pocket (EBP). In order to obtain an optimal template for modeling the structure of the m5-HTR2B, the reference protein structure was initially refined by replacing residues 195-206 of the partially unresolved extracellular loop ECL2 with the corresponding residues belonging to the X-ray structure of h5-HTR2B in complex with methysergide (PDB code 6DRZ), in which the loop was fully solved (McCorvy et al., 2018). All protein residues that did not belong to h5-HTR2B were removed, while the missing side chains of partially unresolved h5- HTR2B residues were automatically reconstructed by using Modeller software (Webb and Sali, 2016). The refined structure was eventually subjected to energy minimization in explicit water environment, after being embedded in a lipid bilayer. The generation of the phospholipid bilayer composed of POPC (1-palmitoyl-2-oleoyl-sn-glycero-3-phosphocholine) molecules and the insertion of the receptor within it were performed using Visual Molecular Dynamics (VMD) software (Humphrey et al., 1996). The energy minimization was then carried out with AMBER software, version 16 (Case. et al., 2016). The system was solvated with a 15 Å water cap on both the “intracellular” and the “extracellular” sides using the TIP3P solvent model, while sodium ions were added as counterions to neutralize the system. The Lipid14 parameters were assigned to POPC molecules. Three sequential minimization stages, each consisting of 5000 steps of steepest descent followed by conjugate gradient, were thus performed. In the first stage, a position restraint of 100 kcal/mol·Å^2 was applied to the whole protein and phospholipid bilayer in order to uniquely minimize the positions of the water molecules. In the

second stage, the same position restraint was only applied to the protein residues, thus leaving the phospholipid molecules free, while in the last stage only the protein α-carbons were restrained with a harmonic potential of 30 kcal/mol·Å^2. The refined h5- HTR2B structure was then used as a template for modelling the structure of m5- HTR2B using Modeller software. A total of 100 different models of m5- HTR2B were generated based on the refined h5-HT$_{2B}$R structure and the model presenting the best value of DOPE score was then selected and subjected to the same energy minimization protocol applied to the template structure. The energy minimized structure was thus considered as the final m5-HTR2B model, which was used for docking and molecular dynamics (MD) simulation studies.

Protein-RNA docking studies. The 3D structure of the murine miRNA-203b-3p core was automatically built, directly from its sequence, using the modeling webserver RNAComposer (Popenda et al., 2012). The generated miRNA core was then docked into the energy minimized model of m5-HT2BR using gold software with PLP fitness function (Verdonk et al., 2003). Considering the dimensions of the miRNA core sequence, in order to take into account a proper portion of the receptor for the docking calculations, including both the supposed OBP and the EBP, the docking site was manually defined based on a selected series of residues. The residues defining the binding site included the homolog residues of h5- HTR2B located in a range of 10 Å form the tripeptide portion of ergotamine in the reference complex (PDB code 4IB4) and the remaining extracellular portions of the receptor. A total of 100 different docking solutions were generated by the docking procedure. The predicted binding orientations of the miRNA core were then visually inspected and filtered according to different criteria. Initially, unreliable binding modes in which the miRNA core protruded into regions that should be occupied by the phospholipid membrane surrounding the protein were discarded. Similarly, docking solutions in which the disposition of the miRNA core was not consistent with the presence of the additional ribonucleotides of the full miRNA sequence were discarded as well. The retained binding modes were then further analyzed in order to select those in which the miRNA core sufficiently occupied the binding site of the receptor. For this purpose, we selected all docking solutions in which the miRNA core presented at least one atom in the range of 5 Å from L361. This residue, located in EBP, is the conserved homolog residue of L362 in h5-HT2BR, which was found to be an interaction site essential for the agonist effect of LSD and responsible of an auxiliary mechanism of agonist activation of h5-HTR2B via the EBP (McCorvy et al., 2018). For this reason, the proximity of the miRNA core to this residue was used as a criterion for selecting reliable binding modes consistent with receptor activation, in which the miRNA core sufficiently occupied at least the EBP of the receptor. By using these filters, 22 reliable binding dispositions were eventually selected and considered for further analyses.

Molecular dynamics simulations. All molecular dynamics (MD) simulations were carried out with AMBER 16. The 22 RNA-protein complexes generated by docking were inserted in a lipid bilayer of POPC molecules and solvated with a 15 Å water cap on both the "intracellular" and the "extracellular" sides, as performed for the above-described energy minimization. TIP3P was used as solvent model, including sodium ions to neutralize the systems. For each complex, the three sequential minimization steps described above were initially performed. Subsequently, as performed in previous MD protocols applied for studying transmembrane receptors (Bizzarri et al., 2019, De Logu et al., 2019), the temperature of the system was gradually raised from 0 to 300 K through a brief constant-volume MD simulation where a position restraint of 30 kcal/mol·Å^2 was applied on the protein α-carbons. The system was then relaxed through a 500 ps constant-pressure MD simulation in which the harmonic potential applied to the protein α-carbons was decreased to 10 kcal/mol·Å^2 and Langevin thermostat was used to maintain the temperature at 300 K. Finally, 25 ns of constant-pressure MD simulation production were performed using the Monte Carlo barostat with anisotropic pressure scaling. In this MD stage, the position restraints on the protein extracellular loops were removed, so that they could fully adapt their conformation to the bound miRNA core. For each complex, the stability of the miRNA core binding conformation during the production stage of the MD simulation was analyzed in terms of root-mean-square deviation (RMSD) of the miRNA phosphorous atoms. The results showed that in few cases the miRNA core partially detached from the protein, completely losing the initial binding mode predicted by docking, as highlighted by an average RMSD value above 10 Å (Table S4). An additional MD production stage of 25 ns, was then performed for the 11 complexes in which the average root-mean-square deviation (RMSD) of the miRNA phosphorous atoms during the MD, with respect to their initial disposition, did not exceed the value of 6.0 Å. The other complexes were instead discarded. The RMSD analysis was then repeated for the 11 complexes considering the full simulation time of 50 ns: in this case, only four complexes (with average miRNA RMSD > 6.0 Å) were discarded (Table S2) and the remaining 7 complexes were selected for binding energy evaluations. All simulations were performed using particle mesh Ewald electrostatics with a cutoff of 10 Å for non-bonded interactions and periodic boundary conditions. A simulation step of 2.0 fs was employed, as all bonds involving hydrogen atoms were kept rigid using SHAKE algorithm. The Lipid14 parameters were assigned to POPC molecules, while RNA.OL3 parameters were used for the miRNA core.

Binding energy evaluations. The evaluation of the binding energy associated with the 7 most reliable miRNA–protein complexes analyzed through MD simulations was carried out using AMBER 16, as

previously described (Poli et al., 2018, Tuccinardi et al., 2007). The trajectories relative to the last 20 ns of each simulation were extracted and used for the calculation, for a total of 200 snapshots (at time intervals of 100 ps). Van der Waals electrostatic and internal interactions were calculated with the SANDER module of AMBER 16, whereas polar energies were calculated using the Poisson-Boltzmann methods with the MM-PBSA module of AMBER 16. Dielectric constants of 1 and 80 were used to represent the gas and water phases, respectively, while the MOLSURF program was employed to estimate the non-polar energies.

Supplementary figures

Figure S1. (**a**) Dose-dependent scratching behavior in C57BL/6J mice induced by intradermal (i.d., 10 µl) injection in the nape of the neck of GSK-1016790A (GSK, 1, 10, 100 pmol) or Veh and pretreated (0.5 hr) with HC-067047 (HC-06, 10 mg/kg, i.p.) or Veh. (**b**) Scratching behavior in *Trpv4*$^{+/+}$and *Trpv4*$^{-/-}$ mice induced by GSK (100 pmol, i.d.) or Veh. (**c**) Scratching behavior in C57BL/6J mice induced by mmu-miR-203b-3p (1 nmol, i.d.) or Veh and pretreated (0.5 hr) with HC-06 (10 mg/kg, i.p.) or Veh. (**d**) Typical traces and cumulative data of the Ca^{2+} response in mTRPV4-HEK293 cells exposed to mmu-miR-203b-3p (10 µM) and GSK (10 nM) or Veh in the presence of HC-06 (30 µM) or Veh. (**e**) Ca^{2+} response in hTRPV1-HEK293 cells exposed to hsa-miR-203b-3p (10 µM), 5-HT (1.5 mM), capsaicin (CPS, 1 µM) or Veh, in the presence of capsazepine (CPZ, 30 µM) or Veh. (**f**) Ca^{2+} response in hTRPA1-HEK293 cells exposed to hsa-miR-203b-3p (10 µM), 5-HT (1.5 mM), allyl isothiocyanate (AITC, 10 µM) or Veh, in the presence of HC-030031 (HC-03, 30 µM) or Veh (n=4 independent experiments). (**g**) Scratching behavior in C57BL/6J mice induced by GSK (100 pmol, i.d.) or Veh and pretreated (0.5 hr) with ketanserin (1 mg/kg, i.p.) or Veh. (n = 6-8 mice per group). Dash (-) represents the combination of different vehicles. Mean±SEM. **P* < 0.05 *vs.* Veh; §*P*<0.05 *vs.* GSK, mmu-miR-203b-3p, CPS, AITC. One-way ANOVA, Bonferroni correction.

Figure S2. (**a**) Cumulative PASI score, (**b**) epidermal thickness and (**c**) scratching behavior in C57BL/6J male and female mice at day 7 after imiquimod (IMQ) or vehicle (control, CTL). (n = 6 mice per group). Mean±SEM. **P* < 0.05 *vs.* CTL. One-way ANOVA, Bonferroni correction.

Supplementary Tables

Table S1. Binding free energy values calculated for the seven most stable miRNA-protein complexes using the MM-PBSA method. Values are expressed in kcal/mol. Related to Figure 4.

Complex	MM-PBSA binding energy (kcal/mol)
3	-13.2
5	-33.4
8	-32.3
10	-26.2
11	-78.5
13	-11.7
20	-42.0

Table S2. Average root-mean-square deviation (RMSD) values of the miRNA core phosphorous atoms during the total 50 ns of MD simulation performed for the 11 selected miRNA-protein complexes. Related to Figure 4.

Complex	miRNA RMSD
2	8.2
3	5.9
5	5.5
8	5.5
10	5.7
11	4.4
12	6.5
13	5.9
15	8.6
18	6.5
20	5.7

Table S3. Rat and mouse primers used in this study.

	Sequence (5' to 3')
Rat b-Actin (NM_031144)	F: CCGCGAGTACAACCTTCTTG R: ATACCCACCATCACACCCTG
Rat HTR1A (NM_012585)	F: AAAGAGCACCTTCCTCTG R: AGAGCCACAATGAAAAACG
Rat HTR1B (NM_022225)	F: AAAAGAACTCCCAAAAGGG R: AGGGTGGGTAAATAGAAAGC
Rat HTR1D (NM_012852)	F: AAAGCCACTAAGACATTGG R: CCACGTGAAGAAGTCAAAG
Rat HTR1F (NM_021857)	F: AAAATATACAGAGCAGCAAGG R: AACATGTAGGATGTGGAGAC
Rat HTR2A (NM_017254)	F: ATCTGTAGGTATATCCATGCC R: CACAAAAGAGCCTATGAGAAC
Rat HTR2B (NM_017250)	F: ACAATCATGTTTGAGGCTAC R: CTGAATTGGCTTTTTGATGG
Rat HTR2C (NM_012765)	F: GGGCAATATCAATAGGAGTTTC R: AGGACGTAGATCGTTAAGAAG
Rat HTR3A (NM_024394)	F: CCTCATTGGTGTCTACTTTG R: CTATTCTGTCTAGGACCAGG
Rat HTR3B (NM_022189)	F: CTCTTGATTCCTAGCATCTTC R: GTAAAGAAGACCCCAATCAG
Rat HTR4 (NM_012853)	F: ACTCATGTGCTAAGGGATAC R: CTTAGGACTGGCTTCTTTTC
Rat HTR5A (NM_013148)	F: CAAACTTCCATAACAGCCTC R: CTTTGATATGTTTGGGGACAG
Rat HTR6 (NM_024365)	F: AATGTTGCTTGTGTAGTGTG R: GACAGATTGCTTTCCTACTG
Rat HTR7 (NM_022938)	F: ATATATGCCTTCTTCAACCG R: GTGGTCAGAGTTTTGTCTTAC
Rat TRPV4 (NM_023970)	F: GTTTGAGGGAGAGGAAGGCT R: TCTACGACCTTCCTCCTCCA
Mouse b-Actin (NM_007393)	F: GACCTCTATGCCAACACAGT R: GGAGCAATGATCTTGATCTT
Mouse HTR1A (NM_008308)	F: CTCACCCTCAGTTTCTTTTC R: TCTAAGTCTCCAACCTCTTG
Mouse HTR1B (NM_010482)	F: ACCCTAGGGATCATTTTAGG R: ATGAGGGAGTTAAGATAGCC
Mouse HTR1D (NM_008309)	F: GAATATACAAACACCTCAGAGC R: GTGACCAAGACTCAAAGAATG
Mouse HTR1F (NM_008310)	F: CACCACGGTATTCATTTCTTC R: CATTCGGTTTAACAGTTCCTC

Mouse HTR2A (NM_172812)	F: ATGAAAAGGTTAGCTGTGTG R: CGCAATGTTAAAAGCATCAC
Mouse HTR2B (NM_008311)	F: AGCGTCTTCTGGAATCTAAG R: AAGCAAGTCATCTGCTTTAG
Mouse HTR2C (NM_008312)	F: GTCTGGATTTCACTAGATGTG R: GAAACTCCTATTGATATTGCCC
Mouse HTR3A (NM_001099644)	F: CTCATCAATGAGTTTGTGGAC R: GAAGTTGTAGATGTCAAGGC
Mouse HTR3B (NM_020274)	F: GTGCAAGAATTGTGTTCAAG R: AAAGAAGACCCCAATCAGAG
Mouse HTR4 (NM_008313)	F: GGCATAGTTGATGTGATAGAG R: CTTAGCAGTGACATAGATTCG
Mouse HTR5A (NM_008314)	F: TTATTCTGAGCCCAGTGAG R: ATTCTTCACCTCCACAGC
Mouse HTR6 (NM_021358)	F: CATCTCTCCAGGTCTCTTC R: GGGGATAGATGATAGGGTTC
Mouse HTR7 (NM_008315)	F: GTTTGTGCTACAAAACTGTG R: CTGTTCTGCATTACTTCTTCTC
Mouse TRPV4 (NM_022017)	F: ATGCTTATCGCCCTCATGGGTG R: CAGGGAAGGAACGCTCGATGTC

Table S4. Average root-mean-square deviation (RMSD) values of the miRNA core phosphorous atoms during the 25 ns of MD simulation initially performed for the 22 miRNA-protein complexes.

Complex	miRNA RMSD
1	8.6
2	5.1
3	5.7
4	7.7
5	5.4
6	11.4
7	6.7
8	5.2
9	17.0
10	5.8
11	5.0
12	5.8
13	5.4
14	6.4
15	5.7
16	12.5
17	7.3
18	4.9
19	6.6
20	5.4
21	6.7
22	7.7

References

Bizzarri BM, Botta L, Aversa D, Mercuri NB, Poli G, Barbieri A, et al. L-DOPA-quinone Mediated Recovery from GIRK Channel Firing Inhibition in Dopaminergic Neurons. ACS Med Chem Lett 2019;10(4):431-6.

Case. DA, Betz. RM, Cerutti. DS, T.E. Cheatham I, Darden. TA, Duke. RE, et al. AMBER 16. University of California, San Francisco; 2016.

De Logu F, Li Puma S, Landini L, Tuccinardi T, Poli G, Preti D, et al. The acyl-glucuronide metabolite of ibuprofen has analgesic and anti-inflammatory effects via the TRPA1 channel. Pharmacol Res 2019;142:127-39.

Faul F, Erdfelder E, Lang AG, Buchner A. G*Power 3: a flexible statistical power analysis program for the social, behavioral, and biomedical sciences. Behav Res Methods 2007;39(2):175-91.

Humphrey W, Dalke A, Schulten K. VMD: visual molecular dynamics. J Mol Graph 1996;14(1):33-8, 27-8.

Kilkenny C, Browne WJ, Cuthill IC, Emerson M, Altman DG. Improving bioscience research reporting: the ARRIVE guidelines for reporting animal research. PLoS Biol 2010;8(6):e1000412.

Li F, Adase CA, Zhang LJ. Isolation and Culture of Primary Mouse Keratinocytes from Neonatal and Adult Mouse Skin. J Vis Exp 2017(125).

Luo DQ, Wu HH, Zhao YK, Liu JH, Wang F. Original Research: Different imiquimod creams resulting in differential effects for imiquimod-induced psoriatic mouse models. Exp Biol Med (Maywood) 2016;241(16):1733-8.

McCorvy JD, Wacker D, Wang S, Agegnehu B, Liu J, Lansu K, et al. Structural determinants of 5-HT2B receptor activation and biased agonism. Nat Struct Mol Biol 2018;25(9):787-96.

Morris RJ, Readio N, Boland K, Johnson K, Lad S, Singh A, et al. Isolation of Mouse Epidermal Keratinocytes and Their In Vitro Clonogenic Culture. J Vis Exp 2019(150).

Poli G, Lapillo M, Granchi C, Caciolla J, Mouawad N, Caligiuri I, et al. Binding investigation and preliminary optimisation of the 3-amino-1,2,4-triazin-5(2H)-one core for the development of new Fyn inhibitors. J Enzyme Inhib Med Chem 2018;33(1):956-61.

Popenda M, Szachniuk M, Antczak M, Purzycka KJ, Lukasiak P, Bartol N, et al. Automated 3D structure composition for large RNAs. Nucleic Acids Res 2012;40(14).

Shimada SG, LaMotte RH. Behavioral differentiation between itch and pain in mouse. Pain 2008;139(3):681-7.

Tuccinardi T, Manetti F, Schenone S, Martinelli A, Botta M. Construction and validation of a RET TK catalytic domain by homology modeling. J Chem Inf Model 2007;47(2):644-55.

Verdonk ML, Cole JC, Hartshorn MJ, Murray CW, Taylor RD. Improved protein-ligand docking using GOLD. Proteins 2003;52(4):609-23.

Wacker D, Wang C, Katritch V, Han GW, Huang XP, Vardy E, et al. Structural features for functional selectivity at serotonin receptors. Science 2013;340(6132):615-9.

Webb B, Sali A. Comparative Protein Structure Modeling Using MODELLER. Curr Protoc Protein Sci 2016;86:2 9 1-2 9 37.

Wilson SR, Gerhold KA, Bifolck-Fisher A, Liu Q, Patel KN, Dong X, et al. TRPA1 is required for histamine-independent, Mas-related G protein-coupled receptor-mediated itch. Nat Neurosci 2011;14(5):595-602.

Zimmermann M. Ethical guidelines for investigations of experimental pain in conscious animals. Pain 1983;16(2):109-10.